Eur. Phys. J. D (2004)
DOI: 10.1140/epjd/e2004-00013-7

THE EUROPEAN PHYSICAL JOURNAL D

Numerical simulation for the characterization of operating conditions of RF–RF hybrid plasma torches*

D. Bernardi, V. Colombo[a], E. Ghedini, and A. Mentrelli

Dipartimento di Ingegneria delle Costruzioni Meccaniche, Nucleari, Aeronautiche e di Metallurgia (DIEM) and Centro Interdipartimentale di Ricerca per le Applicazioni della Matematica (CIRAM),Università di Bologna, via Saragozza 8, 40123 Bologna, Italy

Received 23 December 2003
Published online 10 February 2004 –

Abstract. A two-dimensional (r, z) numerical code has been developed to investigate the prominent features of RF–RF hybrid plasma torches with two stages of different diameter. Flow and temperature fields have been calculated within the assumptions of laminar flow and local thermodynamic equilibrium for the optically thin argon plasma operated at atmospheric pressure, taking into full account the electromagnetic interaction between the primary and the secondary stage of the hybrid device. Results from a detailed parametric study for various geometric, gas flow and electric configurations aim at putting into evidence the wide range of operating conditions that can characterize the use of RF–RF hybrid plasma torches for industrial applications, showing also their possibility to give high enthalpy plasma jets with high torch efficiencies. The magnetofluidynamic modelling described in this work can be an effective tool for providing the theoretical framework for a deep understanding of RF–RF hybrid plasma torches and for designing them as suitable sources for chemical processing of materials, when utilized within an integrated approach that would match the induction plasma torch simulation with the RF generator operating conditions to evaluate the total source efficiency for each particular hybrid configuration.

PACS. 52.75.Hn Plasma torches – 52.65.-y Plasma simulation – 52.80.Pi High-frequency and RF discharges

1 Introduction

RF–RF hybrid plasma torches (also known as dual RF–RF or tandem RF [1–5]) are useful devices for a wide range of applications, such as reactive plasma deposition and synthesis of ultrafine and ultrapure powders. With respect to conventional single-stage RF torches, they provide additional degrees of freedom, which can be exploited in their design for specific applications. In particular, due to the presence of two stages of different diameter and two separated induction coils, RF–RF hybrid plasma sources are characterized, with respect to conventional RF sources by a strong modification of the recirculating flow of plasma gas and by a longer contact between the high temperature zone and the injected materials, impacting favourably the problems of reactant conversion and entrapment, together with the possibility to give higher efficiencies for practical processing [3,4]. In addition, the presence of two induction stages allows one to mix the flow of high-temperature gas leaving the primary stage (primary gas flow rate, signed $Q_1 = Q_{1plasma} + Q_{1sheath}$ in Fig. 1, where details of the torch geometry and fixed operating parameters are given) with a different gas axially (or even radially [3]) injected in the secondary stage (secondary gas flow rate, signed Q_2 in Fig. 1). When the hybrid device would be used to assist a process where the enthalpy content and velocity of the output gas must fit design requests, the use of two stages in cascade can be exploited in order to consequently optimize the torch energy efficiency (in the following η_{torch}, i.e. the ratio between the increase of power content of the gas flowing in the device and the discharge power [6,7]). Moreover, RF–RF hybrid plasma torches permit to avoid the shortcomings of impurity contamination originating from electrode erosion when dealing with DC–RF hybrid sources [8,9]: this fact led in the past to propose and study new concepts of thermal plasma sources of RF–RF hybrid type for the production of ultrafine and ultrapure powders of refractory materials [1, 3,4]. The proposed designs were examined experimentally and their effectiveness as strong competitors of conventional RF thermal plasma sources was demonstrated, at least for some specific application. In that frame, also some numerical investigation of RF–RF hybrid devices has been carried out for fixed torch geometry and electric configuration in a narrow range of operating conditions,

* A colour version of the figures is available in electronic form at `http://www.edpsciences.org`

[a] e-mail: `colombo@ciram.ing.unibo.it`

Table 1. Full set of gas flow operating conditions (with corresponding inlet gas velocities) used in calculations.

Q_1 [slpm]			v_{inlet} [m/s]	Q_2 [slpm] – ΔR [mm] – T_2 [K]	v_{inlet} [m/s]
20	$Q_{1plasma}$	3	0.045	20 – 2.5 – 350	0.808
	$Q_{1sheath}$	17	0.332	20 – 5 – 350	0.386
30	$Q_{1plasma}$	4.5	0.068	20 – 7.5 – 350	0.246
	$Q_{1sheath}$	25.5	0.498	20 – 8.75 – 350	0.206
35	$Q_{1plasma}$	5.25	0.079	20 – 10 – 350	0.177
	$Q_{1sheath}$	29.75	0.581	20 – 12.5 – 350	0.136
40	$Q_{1plasma}$	6	0.090	20 – 15 – 350	0.109
	$Q_{1sheath}$	34	0.664	30 – 5 – 350	0.579
50	$Q_{1plasma}$	7.5	0.113	35 – 5 – 350	0.675
	$Q_{1sheath}$	42.5	0.830	40 – 5 – 350	0.772
60	$Q_{1plasma}$	9	0.135	50 – 5 – 350	0.965
	$Q_{1sheath}$	51	0.996	60 – 5 – 350	1.157
65	$Q_{1plasma}$	9.75	0.146	65 – 5 – 350	1.254
	$Q_{1sheath}$	55.25	1.079	100 – 5 – 350	1.929
				150 – 5 – 350	2.894

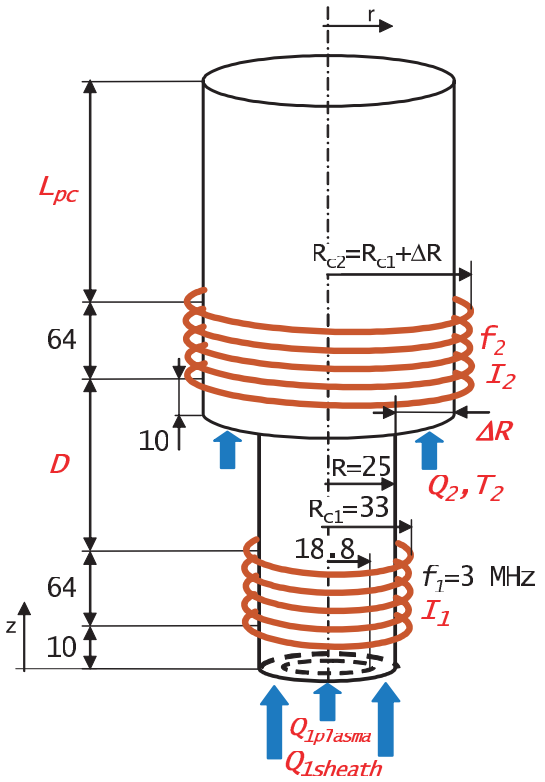

Fig. 1. Scheme of the RF–RF hybrid plasma torch with two stages of different diameter. Dimensions are expressed in millimeters.

also neglecting the electromagnetic interaction between the primary and secondary stage of the torch due to a distance between induction coils of about 90 mm [3]. Our knowledge of the behaviour of these devices seems therefore still far from being complete; their possible future use for applications different from the abovementioned ones (for example, when a plasma jet with high gas flow rate and high enthalpy content is requested for assisting high purity industrial processes) mainly depends upon recognition of the capabilities of these devices to efficiently operate in the wide range of conditions that can be covered by changing design parameters. Therefore, in this work in order to investigate the prominent features of RF–RF hybrid plasma torches, a new numerical code has been developed, starting from a code implemented to study single-stage conventional RF torches, both in steady-state and transient conditions [10,11]. The new code solves the coupled set of two-dimensional (r, z) Navier-Stokes, heat conduction-convection and Maxwell equations, assuming local thermodynamic equilibrium for the optically thin argon plasma operated at atmospheric pressure, while using a grid which extends well outside the torch region for what concerns the electromagnetic field equations with magnetic dipole boundary conditions [10,11]. As conventional one-way conditions do not describe correctly the heat flow phenomena for torch configurations with short post-coil, different boundary conditions for the plasma temperature field at the exit of the torch have been proposed and results have been compared in a test-case conventional RF torch. The interaction between electromagnetic fields of the primary and secondary induction coils has been taken into account under slightly idealized conditions and the results of the new code have been compared with those obtainable by considering the hybrid torch as made of two different stages simulated as separated, non-interfering conventional torches, as done in [3]. A wide set of simulations has been carried out by changing geometric, gas flow (see Tab. 1) and electric parameters, following a strategy of investigation sketched in Figure 5. The aim of the present study being that of highlighting the capabilities of RF–RF hybrid devices over a wide range of possible industrial applications as a result of the wide range of operating conditions that characterize them, only flow and temperature

fields, together with power density distribution and torch energy efficiency, η_{torch}, are analysed: the actual energy efficiency of the RF generators supplying the sources have not been taken into account; that means that to evaluate the overall behaviour and efficiency of the RF–RF source (ratio between net increase of gas enthalpy flux and generator plate power [7,14]) for each particular hybrid configuration, an integrated approach should be followed, matching our model of the induction plasma torch with the RF generators operating conditions in a comprehensive simulation model [12–14].

2 Modelling of RF–RF hybrid plasma torches

2.1 Governing equations

A new numerical code has been developed in order to simulate the behaviour of RF–RF hybrid plasma torches [15–18].

The code solves the two-dimensional (r, z) conservation equations of mass:

$$\frac{\partial \rho}{\partial t} + \frac{1}{r}\frac{\partial}{\partial r}\left(r\rho v_r\right) + \frac{\partial}{\partial z}\left(\rho v_z\right) = 0 \tag{1}$$

r and z-momentum:

$$\rho\left(\frac{\partial v_r}{\partial t} + v_r\frac{\partial v_r}{\partial r} + v_z\frac{\partial v_r}{\partial z}\right) = -\frac{\partial p}{\partial r} + \frac{2}{r}\frac{\partial}{\partial r}\left(\mu r\frac{\partial v_r}{\partial r}\right) + \frac{\partial}{\partial z}\left[\mu\left(\frac{\partial v_r}{\partial z} + \frac{\partial v_z}{\partial r}\right)\right] - \frac{2\mu v_r}{r^2} + G_r \tag{2}$$

$$\rho\left(\frac{\partial v_z}{\partial t} + v_r\frac{\partial v_z}{\partial r} + v_z\frac{\partial v_z}{\partial z}\right) = -\frac{\partial p}{\partial z} + 2\frac{\partial}{\partial z}\left(\mu\frac{\partial v_z}{\partial z}\right) + \frac{1}{r}\frac{\partial}{\partial r}\left[\mu r\left(\frac{\partial v_z}{\partial r} + \frac{\partial v_r}{\partial z}\right)\right] + G_z \tag{3}$$

and energy:

$$\rho\left(\frac{\partial h}{\partial t} + v_r\frac{\partial h}{\partial r} + v_z\frac{\partial h}{\partial z}\right) = \frac{1}{r}\frac{\partial}{\partial r}\left(r\frac{k}{c_p}\frac{\partial h}{\partial r}\right) + \frac{\partial}{\partial z}\left(\frac{k}{c_p}\frac{\partial h}{\partial z}\right) + Q_j - Q_r \tag{4}$$

for the plasma, together with Maxwell equations for the evaluation of the electromagnetic field induced by the coil of the primary stage (*primary coil*):

$$\nabla \times \mathbf{B}^1 = \mu_0\left(\sigma\mathbf{E}^1 + \mathbf{J}^1\right) \tag{5}$$

$$\nabla \times \mathbf{E}^1 = -\frac{\partial \mathbf{B}^1}{\partial t} \tag{6}$$

and of the one induced by the coil of the secondary stage (*secondary coil*):

$$\nabla \times \mathbf{B}^2 = \mu_0\left(\sigma\mathbf{E}^2 + \mathbf{J}^2\right) \tag{7}$$

$$\nabla \times \mathbf{E}^2 = -\frac{\partial \mathbf{B}^2}{\partial t} \tag{8}$$

being G_r and G_z the radial and the axial components of the Lorentz force, respectively; Q_j the Joule heating rate; Q_r the plasma radiation losses; $\mathbf{J}^1$ and $\mathbf{J}^2$ the current densities in the primary and secondary coil, respectively. The set of coupled equations (1–8) is solved by using a finite-volume method based on the SIMPLER algorithm [19] and a fully-implicit method for time discretization. All the calculations have been carried out by assuming that no phase difference exists between the electric currents flowing in the primary and in the secondary coil, even when supplied by different RF generators, which are to be considered perfectly synchronized. Under this assumption, once evaluated the electromagnetic fields induced by the primary and secondary coil ($\mathbf{B}^1$, $\mathbf{E}^1$ and $\mathbf{B}^2$, $\mathbf{E}^2$, respectively) the total magnetic and the total electric fields are obtained by superposition effect:

$$\mathbf{B} = \mathbf{B}^1 + \mathbf{B}^2 \tag{9}$$

$$\mathbf{E} = \mathbf{E}^1 + \mathbf{E}^2 \tag{10}$$

and the radial and axial components of the Lorentz force look like this:

$$G_r = \begin{cases} \frac{1}{2}\sigma\left[E_\theta^1 + E_\theta^2\right]\left[B_z^1 + B_z^2\right] & \text{when } f_1 = f_2 \\ \frac{1}{2}\sigma\left(E_\theta^1 B_z^1\right) + \frac{1}{2}\sigma\left(E_\theta^2 B_z^2\right) & \text{when } f_1 \neq f_2 \end{cases} \tag{11}$$

and

$$G_z = \begin{cases} -\frac{1}{2}\sigma\left[E_\theta^1 + E_\theta^2\right]\left[B_r^1 + B_r^2\right] & \text{when } f_1 = f_2 \\ -\frac{1}{2}\sigma\left(E_\theta^1 B_r^1\right) - \frac{1}{2}\sigma\left(E_\theta^2 B_r^2\right) & \text{when } f_1 \neq f_2 \end{cases} \tag{12}$$

while the Joule heating rate looks as follows:

$$Q_j = \begin{cases} \frac{1}{2}\sigma\left(E_\theta^1\right)^2 + \frac{1}{2}\sigma\left(E_\theta^2\right)^2 + \sigma\left(E_\theta^1 E_\theta^2\right) & \text{when } f_1 = f_2 \\ \frac{1}{2}\sigma\left(E_\theta^1\right)^2 + \frac{1}{2}\sigma\left(E_\theta^2\right)^2 & \text{when } f_1 \neq f_2 \end{cases} \tag{13}$$

being σ the plasma electrical conductivity; E_θ^1 and E_θ^2 the tangential components of the electric fields; B_r^1, B_r^2 and B_z^1, B_z^2 the radial and axial components of the magnetic fields, respectively (the axial and radial components of the electric fields and the tangential components of the magnetic fields being zero because of the axial symmetry).

2.2 Boundary conditions

Equations (1–4) are subject to the boundary conditions shown in Figure 2. Conditions of axial symmetry are applied along the torch axis; the outer wall of the torch is supposed to be at fixed temperature ($T_0 = 350$ K); no-slip and no mass transfer conditions are imposed on the inner quartz wall of the confinement tube (width $s_w = 2$ mm) of both stages of the torch. The *primary gas* is assumed to be injected in the torch at fixed temperature (T_0), with a flat velocity profile at the entrance and consisting of two parts: the plasma gas ($Q_{1plasma}$) and the sheath gas ($Q_{1sheath}$), being the latter the 85% of the total (see also Figs. 1

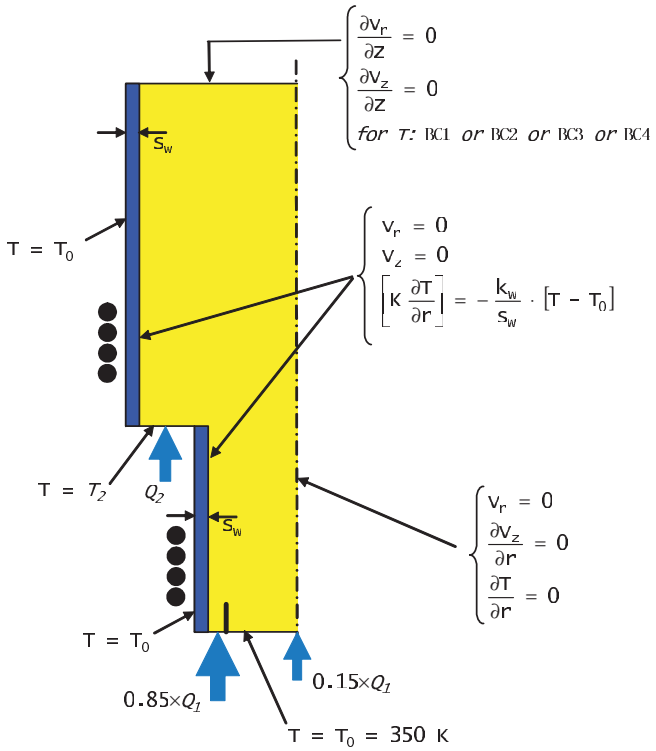

Fig. 2. Schematic view of the boundary conditions for equations (1–4).

and 2). Also the velocity profile of the gas at the secondary torch inlet (*secondary gas*, Q_2, introduced at temperature T_2) is assumed to be flat. All the gas flows at the torch inlets are without swirl components. The gas flow operating conditions for the RF–RF hybrid torch are summarized in Table 1, where also inlet gas velocities (v_{inlet}) corresponding to the primary and secondary gas flow rates are shown. The primary sheath gas is axially injected through an annular gap of width 6.2 mm (see Fig. 1). The secondary gas in axially injected through an idealized annular gap of width ΔR just above the primary stage of the torch: this representation, within a 2–D model, is justified when the real torch geometry is characterized by a relatively high number of gas injection ports [20].

Four different boundary conditions for the plasma temperature at the exit of the torch (see Fig. 2) have been implemented and their effect compared in a test-case calculation:

- *one–way boundary condition* (from now on designated as `BC1`). This imposition relies on the hypothesis of heat convection prevailing over conduction at the exit of the torch (i.e. the Peclet number is *large*);
- $\partial T/\partial z = 0$ (`BC2`). In this case the temperature gradient is assumed to be zero at the exit of the torch. This is the typical imposition of a fully developed flow;
- $\partial^2 T/\partial z^2 = 0$ (`BC3`). In this case the temperature gradient is assumed to be constant at the exit of the torch;
- λ–*boundary condition* (`BC4`). In this case the following plasma temperature profile has been assumed at the exit of the torch:

$$T(r,z) = \vartheta(r)\exp(-\lambda z) + T_0 \tag{14}$$

where λ is a suitable damping parameter [16,18]. The parameter λ is determined by inserting equation (14) into the heat conduction-convection equation and integrating over r at the torch exit. In this way, one obtains the following algebraic equation for λ:

$$a\lambda^2 + b\lambda + c = 0 \tag{15}$$

being

$$\begin{aligned} a &= \int_0^R (T - T_0)\, r dr \\ b &= \int_0^R \frac{c_p}{k}\rho v_z (T - T_0)\, r dr \\ c &= -R\frac{k_s}{k_R}(T_R - T_0) \end{aligned} \tag{16}$$

where c_p, k, ρ are the specific heat, the thermal conductivity and the density of the plasma, respectively; v_z is the axial component of the plasma velocity; k_R, k_s are the plasma and quartz thermal conductivities calculated at the internal surface of the containment tube; T_R is the temperature of the plasma-quartz interface. By taking the z-derivative of the equation (14), the boundary condition:

$$\frac{\partial T}{\partial z} = -\lambda(T - T_0) \tag{17}$$

is obtained, being λ the positive root of equation (15), to be recalculated at each iteration.

In Figure 3, the axial profiles of the plasma temperature obtained by using these four different boundary conditions for a conventional torch in a reference case [21] are shown, for two different lengths of post-coil, while Table 2 presents the evaluated plasma temperature at the torch exit for different radial positions.

The boundary conditions for equations (5–8) are those coming from treating the torch as a magnetic dipole [10,11].

2.3 Computational domain

The governing equations (1–4) are solved using a non-uniform grid for the calculation. In particular, the torch domain is divided into three zones (`A`, `B` and `C`, in Fig. 4a), being the grid uniform within each of them. Details about this grid are given in Figure 4b: in the zooms on the left side the non-uniformity of the grid may be appreciated, while the zooms on the right side carry details of the uniform grid internal to zones `A` and `B`. The number of grid points used to solve equations (1–4) varies from 1290 to 2530, depending on the dimensions of the torch. The primary and secondary coils are treated as idealized axisymmetric regions of radial width 6 mm and

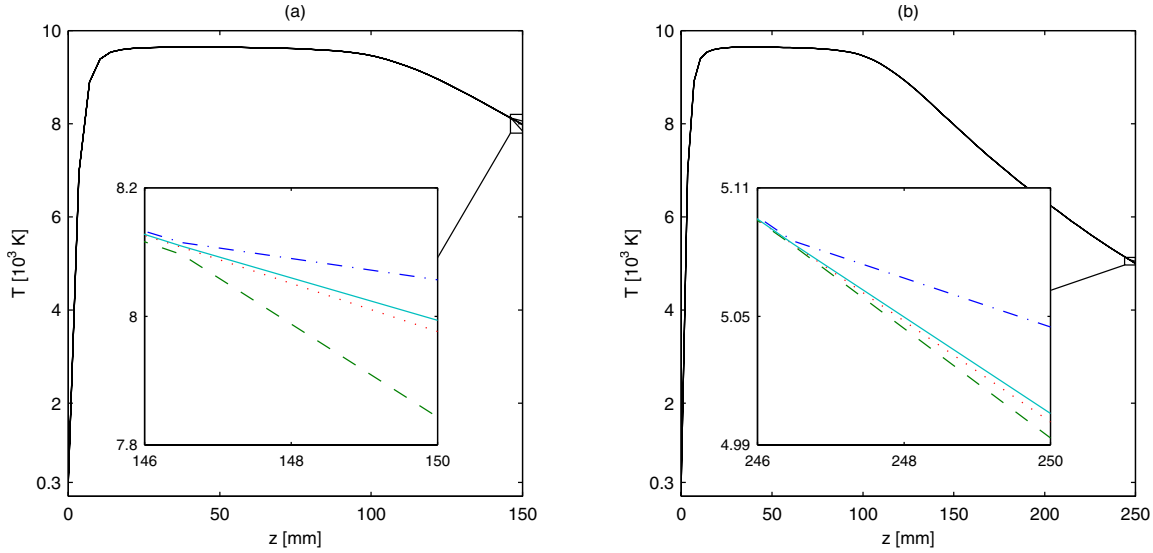

Fig. 3. Effect on axial temperature profile of the four different exit boundary conditions used for the calculation of the temperature field (— BC1; -·-· BC2; ··· BC3; – – BC4) for a conventional torch with the same dimensions as in [21], but with post-coil length of 76 mm (a) and of 176 mm (b). Operating conditions: discharge power = 3 kW; RF generator frequency = 3 MHz; total input gas flow rate = 20 slpm (plasma gas = 3 slpm, sheath gas = 17 slpm).

Table 2. Effect of the four different exit boundary conditions used for the calculation of the temperature field on the plasma temperature [K] at the exit of a conventional torch with the same dimensions as in [21], but with two different post-coil lengths (76 mm and 176 mm), for different radial positions. Operating conditions are in the caption of Figure 3.

	L_{pc} = 76 mm				L_{pc} = 176 mm			
r [mm]	BC1	BC2	BC3	BC4	BC1	BC2	BC3	BC4
0	7994.0	8056.9	7976.3	7843.2	5004.6	5045.1	5000.8	4993.3
5	7832.3	7894.6	7814.0	7677.1	4863.3	4902.5	4859.0	4852.1
10	7312.7	7374.7	7293.1	7152.5	4433.6	4468.9	4427.7	4422.9
15	6280.1	6343.4	6258.0	6130.0	3691.2	3719.7	3682.8	3681.7
20	4430.1	4476.7	4400.3	4310.6	2553.8	2572.1	2542.6	2546.9
25	424.8	425.2	424.3	423.0	379.5	379.5	379.3	379.3

height 64 mm where the currents flow orthogonally to r- and z-directions with imposed linear densities I_1 and I_2.

Maxwell equations (5–8) are solved on a computational domain extending well outside the torch region, as shown if Figure 4b. The grid adopted for the evaluation of the electromagnetic field induced by the primary coil is the one represented on the left, while the one used for the evaluation of the electromagnetic field induced by the secondary coil is shown on the right. The grids are highly non-uniform, in order to permit an optimization of the computational effort.

3 Selected results

In order to characterize the RF–RF hybrid torch (sketched in Fig. 1), a newly–developed, fully 2D (r, z) fluid–magnetic code [16,18] has been employed and a wide set of numerical simulations has been carried out, following the strategy of investigation depicted in Figure 5. A detailed parametric study has been performed by changing geometric, flow and electric parameters. Geometric parameters include:

- the distance between the two induction coils, D;
- the difference between the radii of the two stages of the torch, ΔR;
- the length of the post-coil region of the secondary stage of the torch, L_{pc}.

Flow parameters include:

- the primary gas flow rate, Q_1 (equal to the sum of the plasma gas flow rate, Q_{plasma}, and the sheath gas flow rate, Q_{sheath});
- the secondary gas flow rate, Q_2;
- the inlet temperature of the secondary gas, T_2.

Finally, electric parameters include:

- the frequency of the secondary coil, f_2;
- the primary linear coil current density, I_1;
- the secondary linear coil current density, I_2.

At this stage of the investigation, other dimensions and operating conditions are fixed and the corresponding values are given in Figure 1.

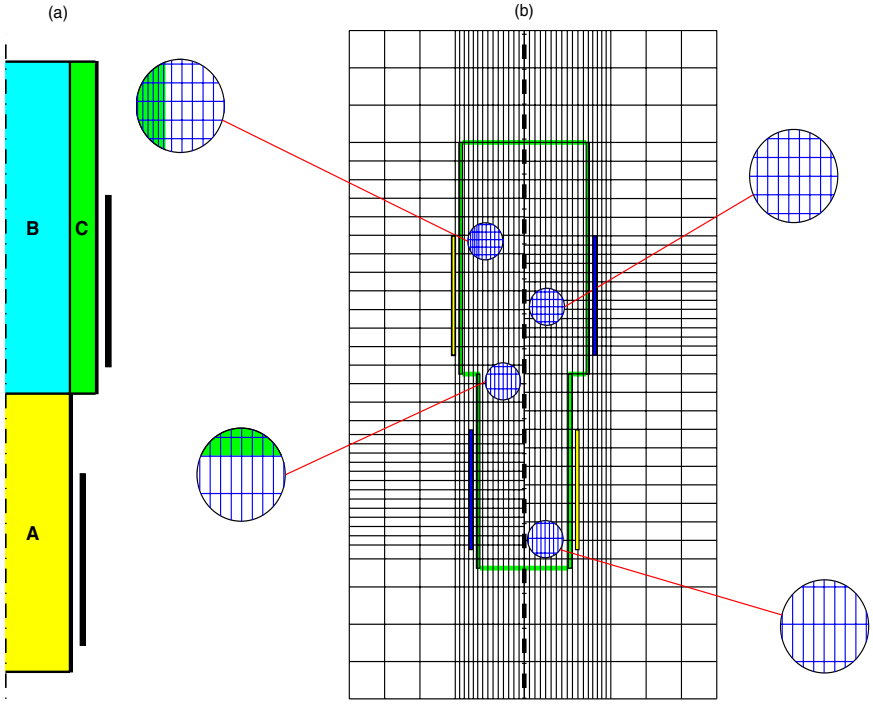

Fig. 4. (a) The grid system used for temperature and flow fields calculation is non–uniform over the whole computational domain, but is uniform within each of the three zones (`A`, `B` and `C`) shown here. (b) Sketch of the computational domain. The grid on the left (right) is the one adopted for the evaluation of the electromagnetic field induced by the coil of the primary (secondary) stage. Details of the grid used for the calculation of the temperature and flow fields inside the torch are shown in the zoomed particulars.

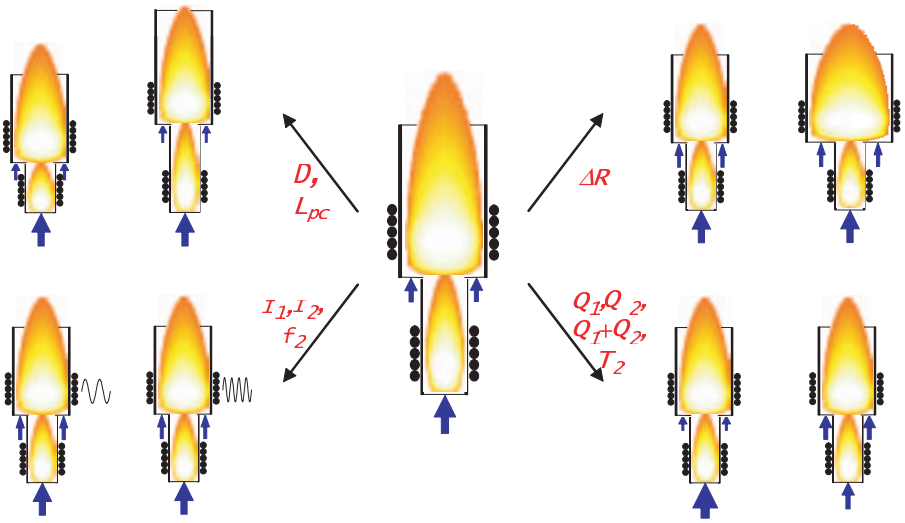

Fig. 5. Strategies of investigation of prominent features of RF–RF hybrid plasma torches: parametric study has been performed by changing D, distance between coils; ΔR, difference between the radii of the two torches; f_2, secondary coil current frequency; I_1 and I_2, primary and secondary linear coil current densities; Q_1 and Q_2, primary and secondary gas flow rates; T_2, secondary gas inlet temperature; L_{pc}, length of the post-coil region of the secondary stage.

Before presenting a selection of the great amount of available simulation results, definitions of the adopted symbols employed in the report are given.

In the following, P is the discharge power, i.e. the power dissipated in the discharge:

$$P = \int_V Q_j dV$$

being V the region occupied by the plasma and Q_j the density distribution of the power dissipated in the discharge; ΔP_{gas} is the difference between the power content of the gas at the exit of the torch and the power content of the primary and secondary gas at the torch inlets:

$$\Delta P_{gas} = P_{gas}^{exit} - P_{gas}^{inlet}$$

where

$$P_{gas}^{exit} = \int_0^{R+\Delta R} \rho\left(r, z_e\right) v_z\left(r, z_e\right) h\left(r, z_e\right) 2\pi r dr$$

and

$$P_{gas}^{inlet} = \int_0^{R} \rho\left(r, z_{i1}\right) v_z\left(r, z_{i1}\right) h\left(r, z_{i1}\right) 2\pi r dr + \int_R^{R+\Delta R} \rho\left(r, z_{i2}\right) v_z\left(r, z_{i2}\right) h\left(r, z_{i2}\right) 2\pi r dr$$

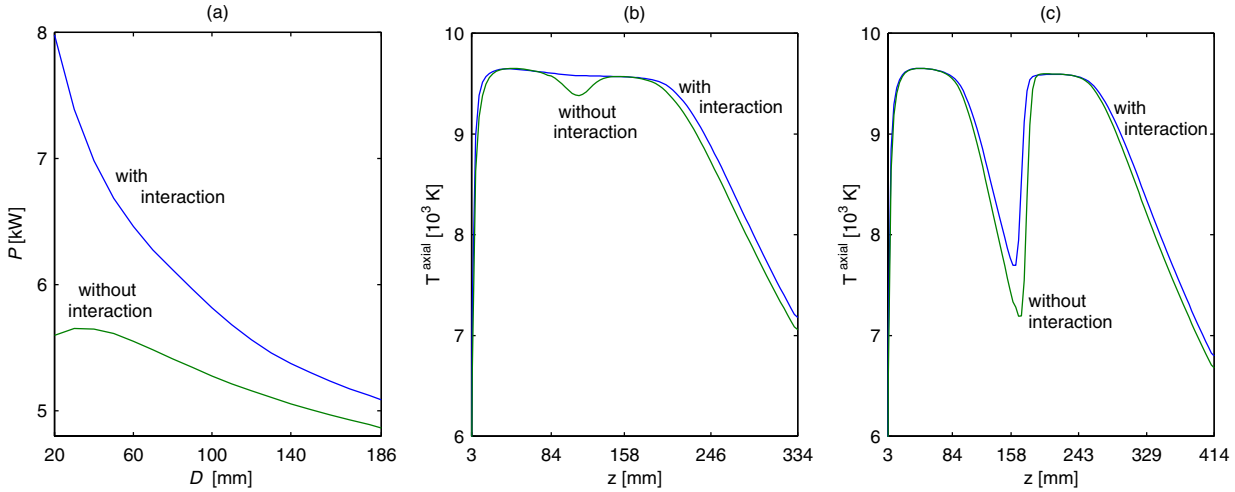

Fig. 6. Effect of interaction between the two stages of different diameter for the RF–RF hybrid plasma torch; $\Delta R = 5$ mm, $I_1 = 4600$ A/m, $I_2 = 4300$ A/m, $f_2 = 3$ MHz, $Q_1 = Q_2 = 20$ slpm, $T_z = 350$ K, $L_{pc} = 100$ mm. (a) Discharge power as a function of the distance, D, between coils; (b, c) axial profiles of the plasma temperature for the cases with $D = 20$ mm and $D = 100$ mm, respectively.

being ρ, v, h the density, velocity and enthalpy of the gas, respectively, while z_e, z_{i1} and z_{i2} are the z coordinates of the exit of the torch and of the primary and secondary inlets.

The efficiency of the torch, η_{torch}, is defined as

$$\eta_{torch} = \Delta P_{gas}/P \times 100$$

while the average plasma jet enthalpy, $h_{s,exit}$, is to be intended as the ratio between the power content of the gas at the exit of the torch and the total argon mass flow rate $(Q_1 + Q_2)$ [7]:

$$h_{s,exit} = P_{gas}^{exit}/(Q_1 + Q_2).$$

The quantities $q_{w,1}$ and $q_{w,2}$ are the maximum heat fluxes through the quartz confinement tube of the primary and secondary stage of the hybrid torch, respectively.

The values of the physical quantities described above are given at the bottom of the figures for all the cases for which plasma temperature and flow fields are presented (Figs. 7, 10, 16, 22, 25, 28 and 19).

Finally, the flow field in the torch is visualized by means of arrows in Figures 7, 10, 16, 22, 25, 28, 19 (each arrow representing the velocity vector of the gas), and by means of streamlines in Figures 8, 11, 17, 23, 26, 29, 20. The difference between the values reported in the labels of two adjacent streamlines represents the fraction of the gas injected in the torch $(Q_1 + Q_2)$ flowing in the region enclosed within those two streamlines (being a streamline tangent to the gas velocity vector); also the values of the axial component of the gas velocity along the streamlines at the exit of the torch are locally reported.

Most of the results that will be presented in the following sections refer to torch geometrical configurations with post-coil length $L_{pc} = 100$ mm. Some investigation has also been done to consider the effect of values of L_{pc} in the range $L_{pc} = 10 \div 176$ mm to keep into account possible different technological requests on plasma main characteristics P, ΔP_{gas}, η_{torch}.

3.1 Parametric study of geometric configurations

Numerical simulations have been carried out with the aim of putting into evidence the effects on the behaviour of the RF–RF hybrid torch of changing the distance between the two induction coils (D) and the difference between the radii of the two stages of the device (ΔR), for a wide range of gas flow and electric operating conditions. In this section, the results obtained for one representative set of values of gas flow and electric parameters (given in Figs. 7 and 10), fully describing the operating conditions of the hybrid device, are presented. The simulation results show that the value of the distance D between the two induction coils strongly affects the characteristics of the plasma discharge. For distances between the coils in the range from 20 mm to 70 mm, the high temperature region of the discharge spans the region corresponding to the two induction coils and the gap between them, while an increase in D leads to a progressive splitting of the discharge into two different, separate discharges. Plasma temperature and velocity fields, as well as power density distribution in the plasma and streamline patterns are reported in Figures 7 and 8, for a set of values of D ranging from 20 mm to 170 mm, for the case with $\Delta R = 5$ mm. As announced, the geometric configurations with $D = 120$ mm and $D = 170$ mm are characterized by two almost separate discharges and the hybrid torch behaves as a device made up of two separate, independent, conventional torches in cascade. Anyway, even in these configurations, the interaction between the two stages cannot be neglected, even for the highest values of D here taken into consideration. For example, Figures 6b and 6c show the axial profiles of the plasma temperature for the cases with $D = 20$ mm and $D = 100$ mm, taking into account and neglecting

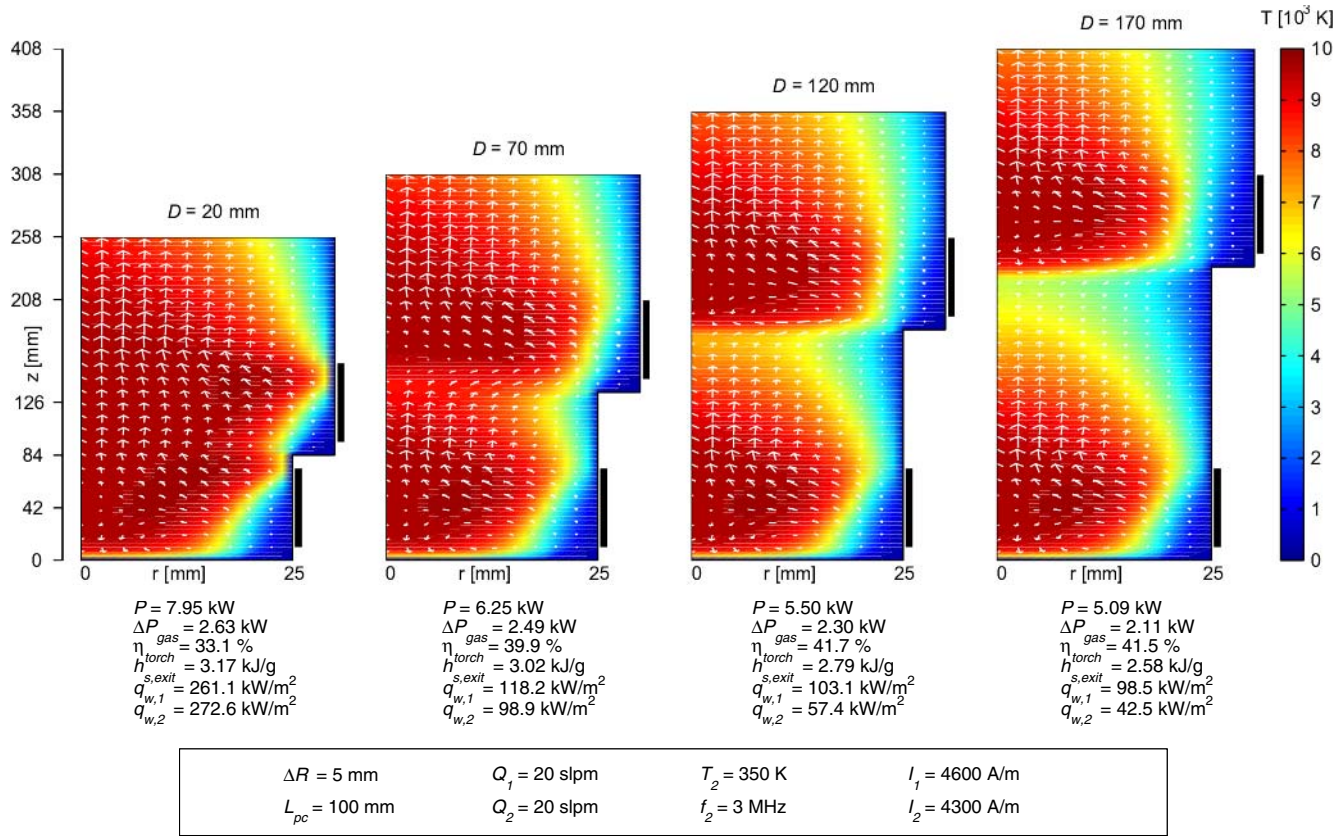

Fig. 7. Plasma temperature and velocity fields for the RF–RF hybrid torch with different values of D.

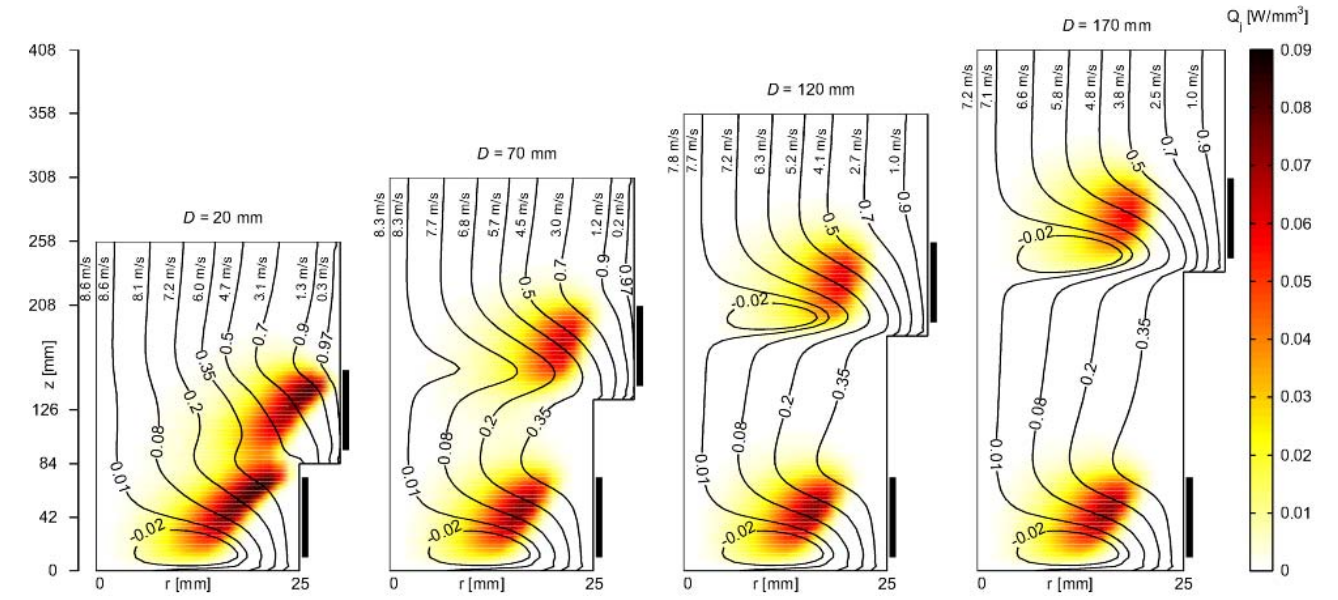

Fig. 8. Power density distributions and streamline patterns, with corresponding axial components of gas velocity at the exit of the RF–RF hybrid torch, for the cases of Figure 7.

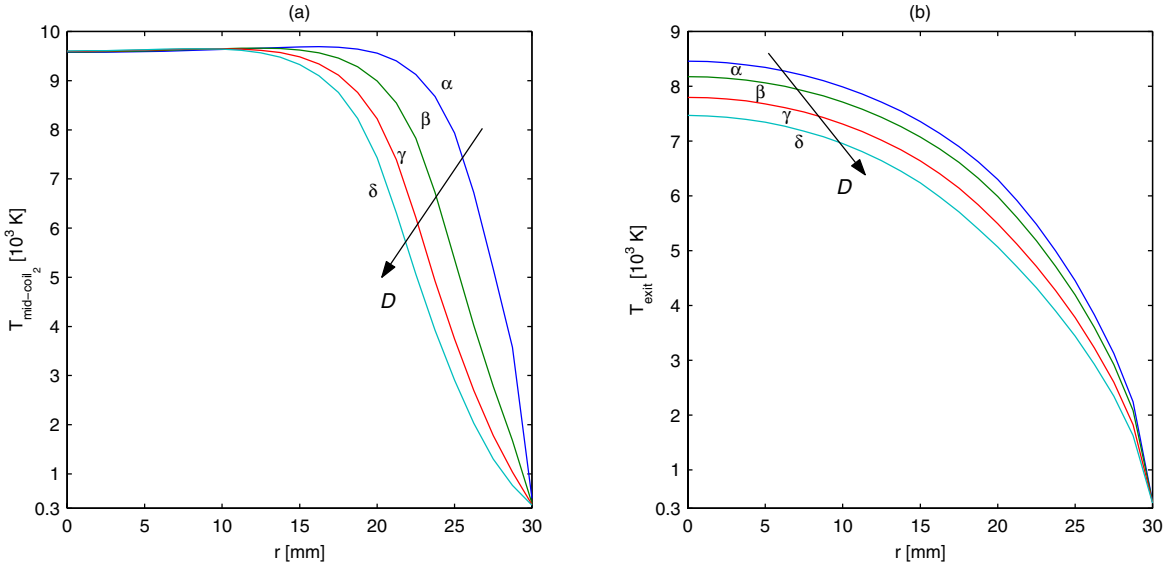

Fig. 9. Radial profiles of plasma temperature at mid-coil of the secondary stage (a) and at the torch exit (b) for the cases of Figure 7: (α) $D = 20$ mm; (β) $D = 70$ mm; (γ) $D = 120$ mm; (δ) $D = 170$ mm.

the interaction between the primary and secondary stages of the RF–RF hybrid torch. The results show that, even when the geometric configuration is characterized by a value of D equal to 100 mm, the hybrid torch cannot be properly considered as made of two different, separated, non-interfering conventional torches (as done in [3]). Moreover, a change in the value of D always implies noticeable changes in the values of both P and ΔP_{gas}, as shown in Figures 6a, 7, 13a and 13b, for the case with interaction between the two stages of the device. In particular, from Figure 6a, one can argue that the discharge power, P, tends to become less and less dependent on the value of D, as the latter increases, approaching a value (depending on the electric and gas flow configurations), that is reached when the interaction between the two stages of the hybrid device becomes negligible. However, for $D \backsim 100$ mm the interaction between the two stages still appears to be important. This conclusion is also supported by Figure 8, where one can appreciate that both the streamline patterns and the power density distribution are strongly affected by a change in the value of D over the whole range of values used for this parameter. For what concerns the fluid-dynamic behaviour of the system, the recirculating vortex that appears in the secondary stage of the torch when $D > 70$ mm gradually grows with D, and the region when the power is mainly dissipated slightly modifies its shape and position. Accordingly, even the size of the high temperature region in the discharge is affected by the values of D, decreasing its radial extension as the value of D increases (see Figs. 7 and 9a). Such a behaviour, for what concerns the secondary discharge, is also responsible for the different radial plasma temperature profiles at the exit of the torch, that can be appreciated in Figure 9b.

From Figures 7 and 13 it can also be seen that η_{torch} reaches a plateau for increasing values of D with a weak dependency on ΔR, all within quite acceptable values of maximum heat flux at the walls of both the primary and the secondary stage of the device. A change in the radial dimension of the secondary stage leads to important modifications in the way power is dissipated in the discharge (as evidenced by Fig. 11), and in the fluid-dynamics of the plasma (Figs. 10 and 11), with noticeable changes both in the velocity magnitude at the exit of the torch and in the streamline patterns of the primary gas, leading, in turn, to quite different dwell time of the primary gas injected in the torch.

Figure 12a, just as Figure 9a did for changing D, shows that the maximum plasma temperature at mid-coil of the secondary stage is not much affected by a change in ΔR, while Figure 12b, unlike Figure 9b for increasing values of D, shows that a slight increase in the maximum plasma temperature at the exit of the device occurs increasing ΔR.

The effect of changing ΔR on the characteristics of the discharge may also be appreciated in Figures 13 and 14, where the dependency of P, ΔP_{gas} and η_{torch} on both D and ΔR is shown. It is worth noticing that the value of η_{torch}, as well as the value of ΔP_{gas}, is strongly dependent on the length of the post-coil region of the secondary stage of the hybrid torch (parameter L_{pc}), as shown if Figure 15 for a wide set of operating conditions of the RF–RF hybrid torch, covering various geometric, electric and gas flow configurations, which will be further discussed in Sections 3.1 and 3.2.

The combined effects on P, ΔP_{gas} and η_{torch} of simultaneously changing the geometric parameters (D and ΔR) and the frequency of the secondary coil current, f_2, are pointed out in Table 3 for a geometric configuration with $L_{pc} = 40$ mm. The simulation results have pointed out that for a frequency f_2 equal to 2 MHz (or lower), the discharge in the secondary stage of the hybrid device cannot be sustained, regardless of the values of D and ΔR. Visualization of the flow and temperature fields, as well as of the power density distribution, in one case ($D = 20$ mm) of

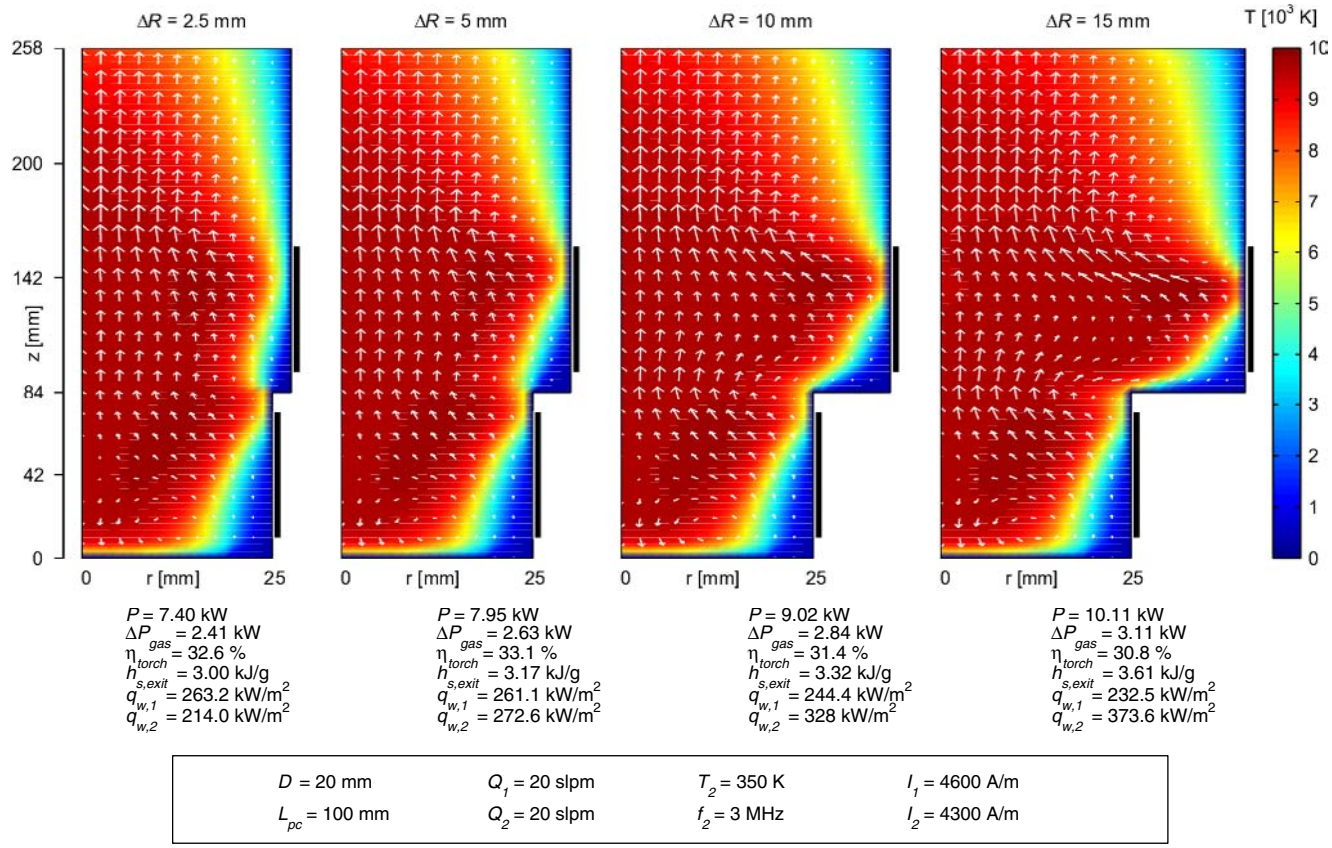

Fig. 10. Plasma temperature and velocity fields for the RF–RF hybrid torch with different values of ΔR.

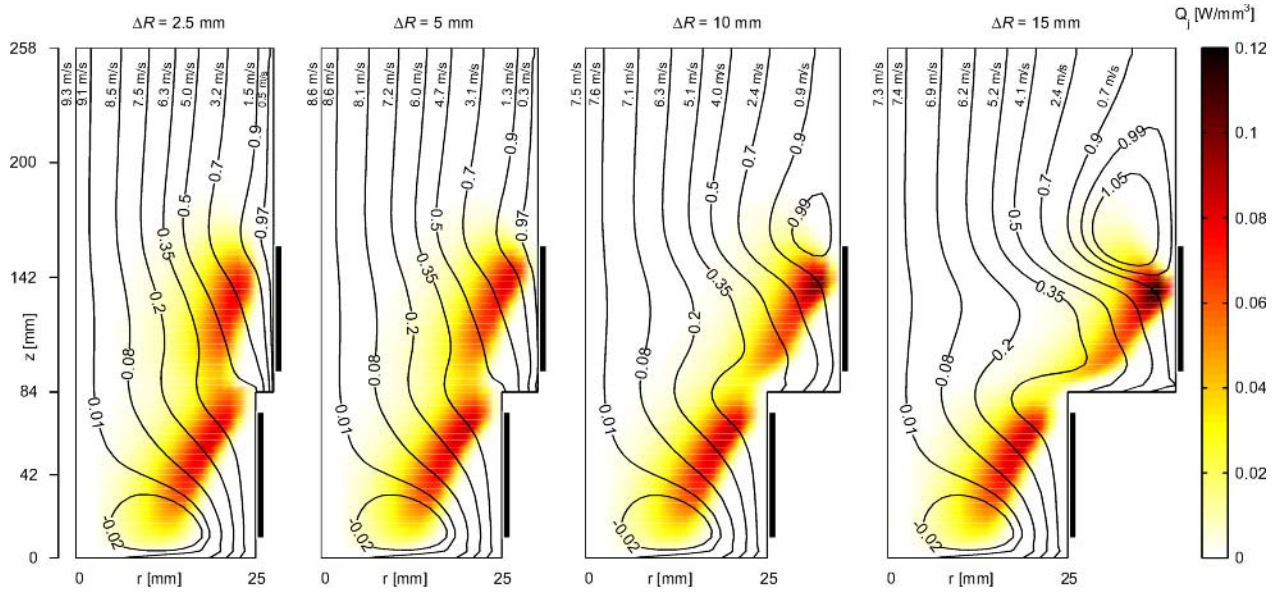

Fig. 11. Power density distributions and streamline patterns, with corresponding axial components of gas velocity at the exit of the RF–RF hybrid torch, for the cases of Figure 10.

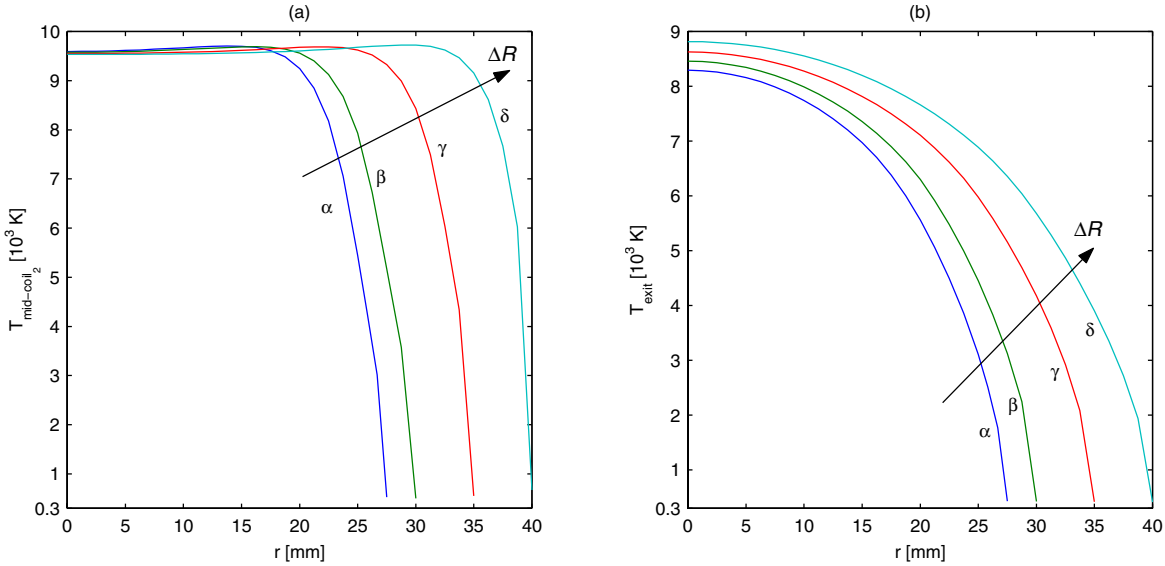

Fig. 12. Radial profiles of plasma temperature at mid-coil of the secondary stage (a) and at the torch exit (b) for the cases of Figure 10: (α) $\Delta R = 2.5$ mm; (β) $\Delta R = 5$ mm; (γ) $\Delta R = 10$ mm; (δ) $\Delta R = 15$ mm.

Table 3. P [kW] (bold), ΔP_{gas} [kW] (italic) and η_{torch} [%] (normal) as function of f_2 for different values of D and ΔR, for the RF–RF hybrid torch with $I_1 = 4600$ A/m, $I_2 = 4300$ A/m, $Q_1 = 20$ slpm, $Q_2 = 20$ slpm, $T_2 = 350$ K, $L_{pc} = 40$ mm; (n.s.) indicates operating conditions where discharge in the secondary stage cannot be sustained.

f_2 [MHz]	$\Delta R = 5$ mm			$\Delta R = 10$ mm			$\Delta R = 15$ mm		
	D [mm]			D [mm]			D [mm]		
	20	60	100	20	60	100	20	60	100
2.0	**(n.s.)**	**(n.s.)**	**(n.s.)**	**(n.s.)**	**(n.s.)**	**(n.s.)**	**(n.s.)**	**(n.s.)**	**(n.s.)**
	(n.s.)	*(n.s.)*	*(n.s.)*	*(n.s.)*	*(n.s.)*	*(n.s.)*	*(n.s.)*	*(n.s.)*	*(n.s.)*
	(n.s.)	(n.s.)	(n.s.)	(n.s.)	(n.s.)	(n.s.)	(n.s.)	(n.s.)	(n.s.)
2.5	**5.4**	**5.2**	**4.9**	**6.1**	**5.7**	**5.1**	**6.9**	**6.4**	**5.5**
	3.3	*2.9*	*2.6*	*3.7*	*3.1*	*2.7*	*4.1*	*3.5*	*2.9*
	60.8	56.2	53.5	59.8	55.1	52.9	58.5	55.0	52.5
3.0	**8.1**	**6.5**	**5.8**	**9.2**	**7.3**	**6.2**	**10.2**	**8.5**	**7.2**
	3.6	*3.3*	*3.0*	*3.8*	*3.7*	*3.2*	*4.1*	*4.1*	*3.7*
	43.8	51.6	52.1	41.8	50.7	52.1	40.7	48.1	51.0
3.5	**6.6**	**6.1**	**6.1**	**7.8**	**7.0**	**6.5**	**8.9**	**8.7**	**8.2**
	3.5	*3.4*	*3.2*	*3.8*	*3.7*	*3.5*	*4.0*	*4.5*	*4.0*
	53.2	55.4	53.0	48.7	52.9	53.6	45.5	52.1	48.6
4.0	**7.2**	**6.7**	**6.6**	**8.3**	**7.6**	**7.2**	**9.5**	**9.3**	**8.9**
	3.5	*3.5*	*3.4*	*3.8*	*3.8*	*3.7*	*4.0*	*4.3*	*4.1*
	49.1	52.9	51.4	45.2	49.6	52.3	42.1	46.1	45.4
4.5	**7.7**	**7.3**	**7.1**	**8.9**	**8.2**	**7.8**	**10.1**	**9.8**	**9.6**
	3.5	*3.6*	*3.5*	*3.7*	*3.8*	*3.9*	*4.0*	*4.1*	*3.9*
	46.1	48.8	49.1	42.2	46.2	49.2	39.4	42.1	40.6

non-sustainability of the discharge in the secondary stage, is given in Figures 16 and 17 for a geometric configuration with $L_{pc} = 100$ mm. It must also be said that, for configurations with such small values of D ($D \backsim 20$ mm), it is not fully correct to distinguish between a primary and a secondary discharge, being the interaction between the two coils not negligible at all. In this situations, non-sustainability of the secondary-stage of the plasma means that when the secondary coil is active without current flowing in the primary coil, the discharge would not sustain itself.

The set of results summarized in Table 3 show that frequency $f_2 = 3$ MHz $= f_1$ play the role of discriminate the behaviour of the device for what concerns η_{torch}: in fact, for $f_2 < 3$ MHz, η_{torch} decreases for increasing D, regardless of the value of ΔR. For $f_2 > 3$ MHz, η_{torch} behaves in a more complicated way: for some choice of ΔR and f_2 ($\Delta R = 5$ mm and $f_2 = 3.5$, 4.0 MHz; $\Delta R = 15$ mm and $f_2 = 3.5$, 4.0, 4.5 MHz) η_{torch} has a maximum in the spanning range of D or either a monotonically increasing behaviour for increasing D ($\Delta R = 10$ mm and $f_2 = 3.5$, 4.0, 4.5 MHz). Values of η_{torch} range from 39.4 up to 60.8

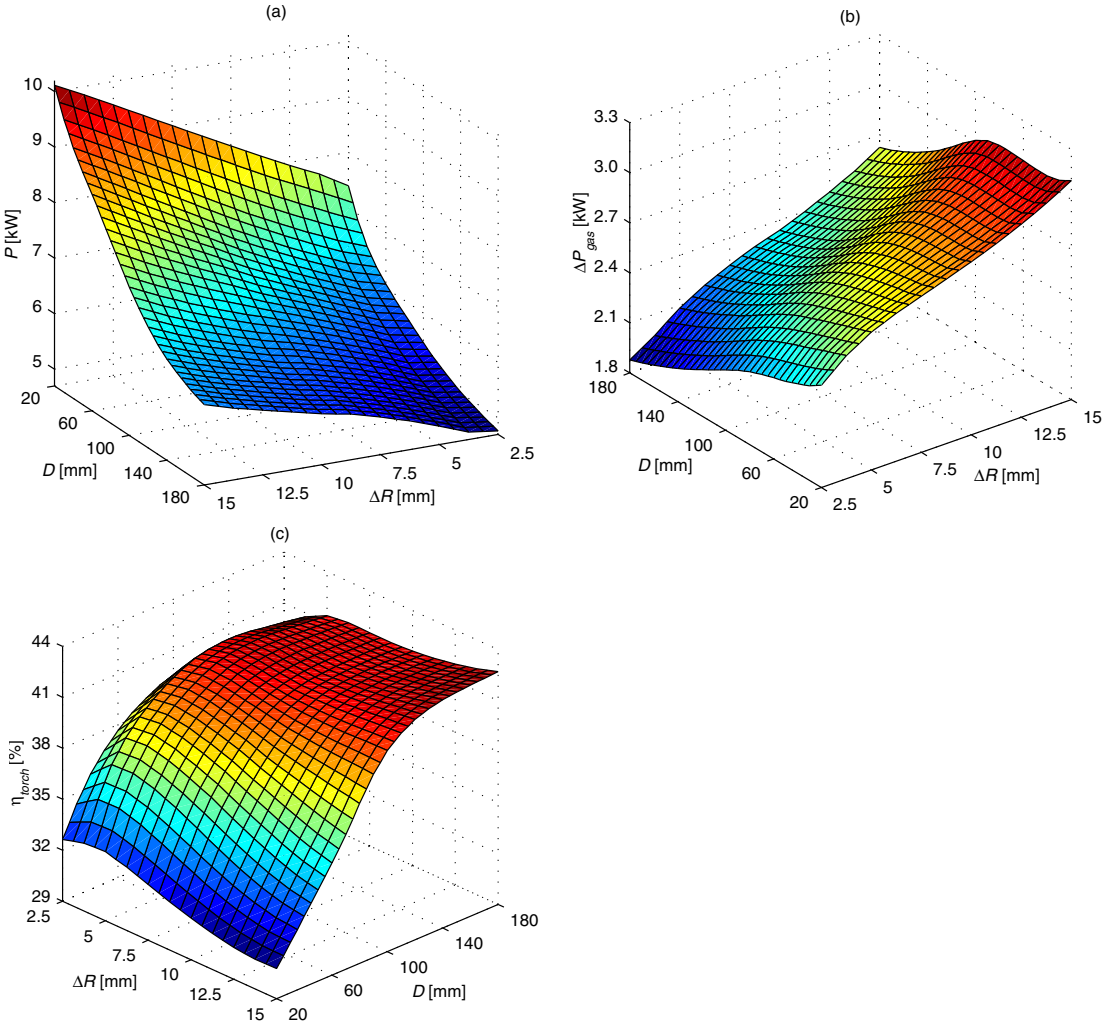

Fig. 13. Effect of changing D and ΔR on P (a), ΔP_{gas} (b), η_{torch} (c), for the RF–RF hybrid torch with the following operating conditions: $Q_1 = Q_2 = 20$ slpm, $T_2 = 350$ K, $f_2 = 3$ MHz, $I_1 = 4600$ A/m, $I_2 = 4300$ A/m, $L_{pc} = 100$ mm.

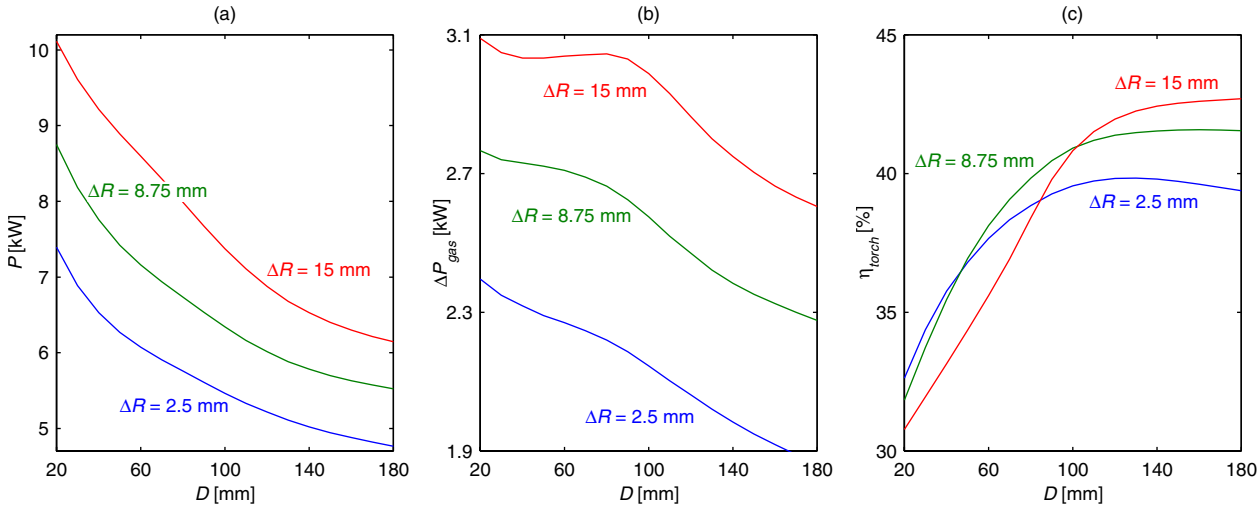

Fig. 14. Effect of changing D and ΔR on P, ΔP_{gas} and η_{torch} for the RF–RF hybrid torch with $Q_1 = Q_2 = 20$ slpm, $f_2 = 3$ MHz, $I_1 = 4600$ A/m, $I_2 = 4300$ A/m, $T_2 = 350$ K, $L_{pc} = 100$ mm.

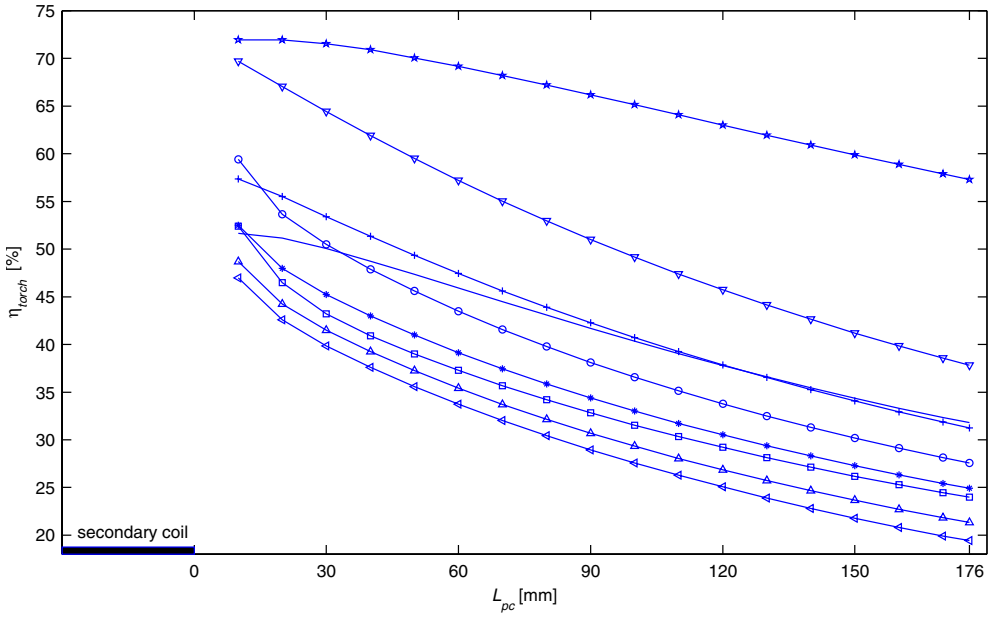

Fig. 15. Efficiency (η_{torch}) of the RF–RF hybrid torch with different values of the post-coil length L_{pc}. Operating conditions for curve ($*$) are: $I_1 = 4600$ A/m, $I_2 = 4300$ A/m, $D = 20$ mm, $\Delta R = 5$ mm, $Q_1 = Q_2 = 20$ slpm, $f_2 = 3$ MHz, $T_2 = 350$ K; for all the other curves the operating conditions are the same of curve ($*$) except but for: ($\triangledown$) $f_2 = 2$ MHz, ($\circ$) $f_2 = 4$ MHz, ($+$) $D = 100$ mm, (solid line) $D = 186$ mm, ($\star$) $Q_1 = 20$ slpm, $Q_2 = 60$ slpm, ($\square$) $\Delta R = 10$ mm, ($\triangle$) $T_2 = 1500$ K, ($\triangleleft$) $T_2 = 2000$ K. All results are obtained imposing exit boundary conditions of type `BC4` for the calculation of the temperature field.

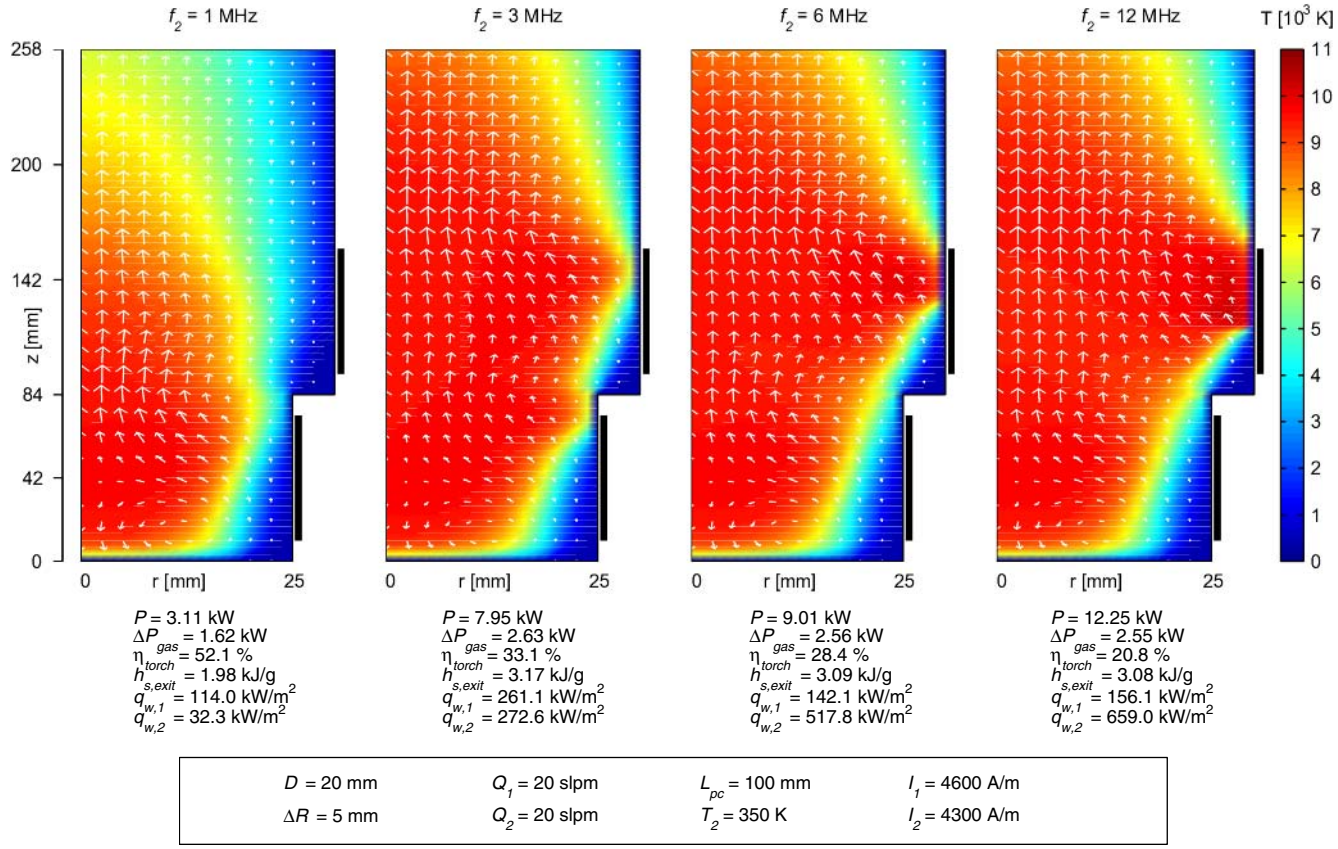

Fig. 16. Plasma temperature and velocity fields for the RF–RF hybrid torch with different values of f_2.

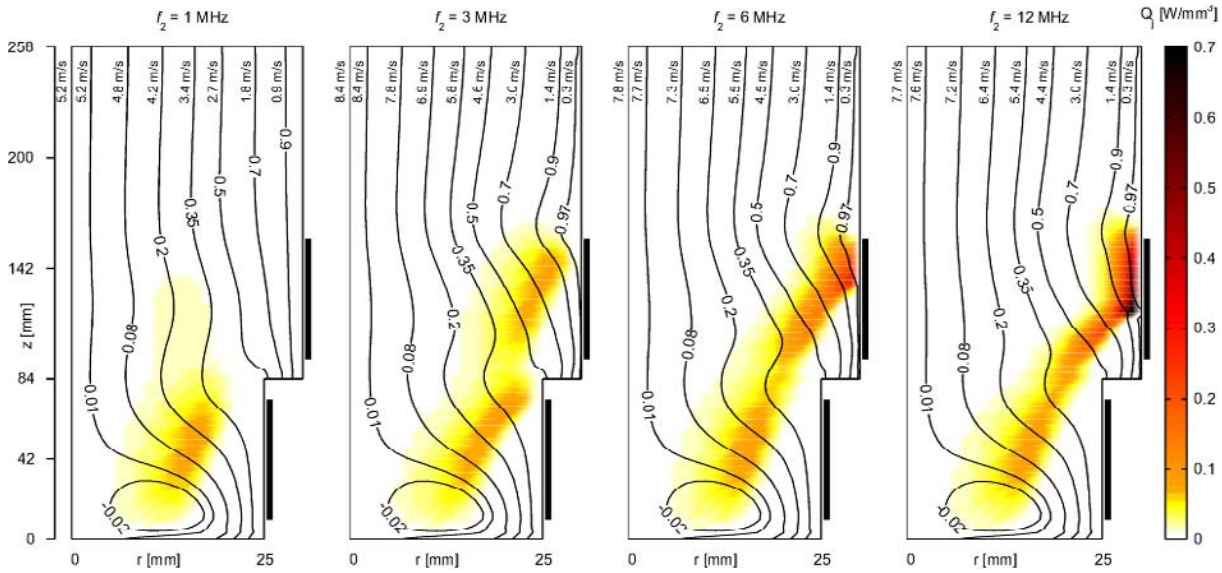

Fig. 17. Power density distributions and streamline patterns, with corresponding axial components of gas velocity at the exit of the RF–RF hybrid torch, for the cases of Figure 16.

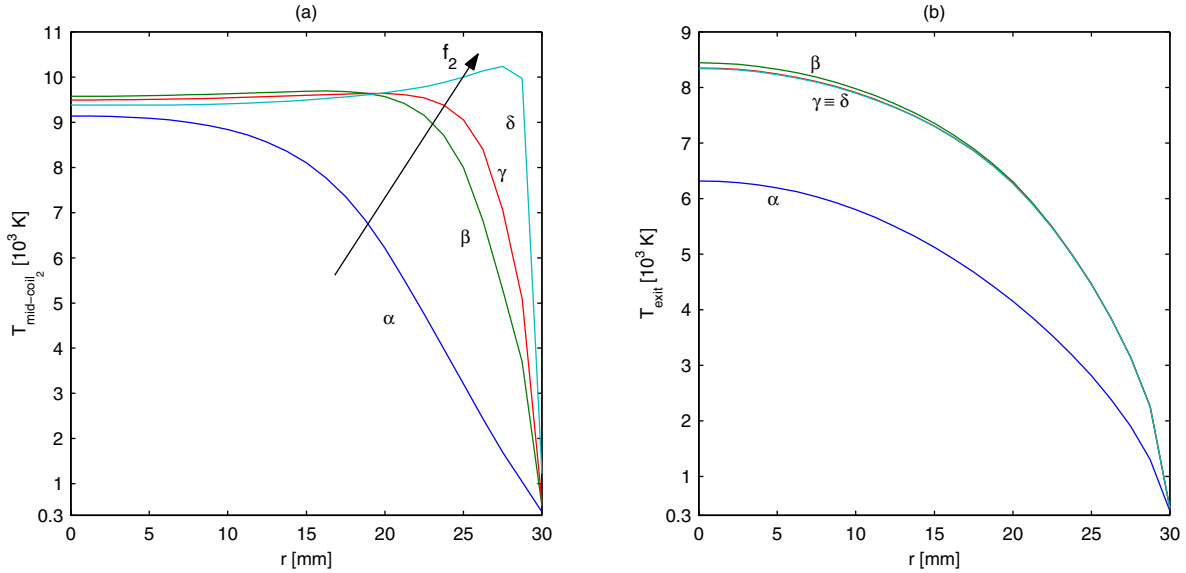

Fig. 18. Radial profiles of plasma temperature at mid-coil of the secondary stage (a) and at the torch exit (b) for the cases of Figure 16: (α) $f_2 = 1$ MHz; (β) $f_2 = 3$ MHz; (γ) $f_2 = 6$ MHz; (δ) $f_2 = 12$ MHz.

in the whole spanning range of f_2, ΔR and D. Discharge power P, for each choice of f_2 and ΔR is always monotonically increasing for increasing D, as already strongly evidenced (for $f_2 = 3$ MHz) in Figure 13a.

3.2 Parametric study of electric configurations

The parametric study has put into evidence that the value of the frequency of the secondary coil current, f_2, drastically affects the plasma temperature field, in particular for what concerns the secondary stage of the hybrid device, as it can be appreciated in Figure 16, where the effects of four different electric configurations with f_2 ranging from 1 MHz to 12 MHz are compared. A strong effect of f_2 on discharge power P and on η_{torch} is shown in the data presented in Figure 16; the strong dependency of P on f_2 is highly related to the way power is dissipated in the discharge: increasing values of f_2 lead to power density distributions (given in Fig. 17), which are more and more localized near the wall of the secondary confinement tube, as expected. The consequent increase of the heat flux through the wall of the secondary stage of the torch, also evidenced in Figure 18a for what concerns plasma temperature in the mid-coil region, may lead, in some configurations, to indesiderably high values of the temperature on the inside wall of the confinement tube, which (in the present configurations for tube geometry, tube material and temperature boundary conditions) can

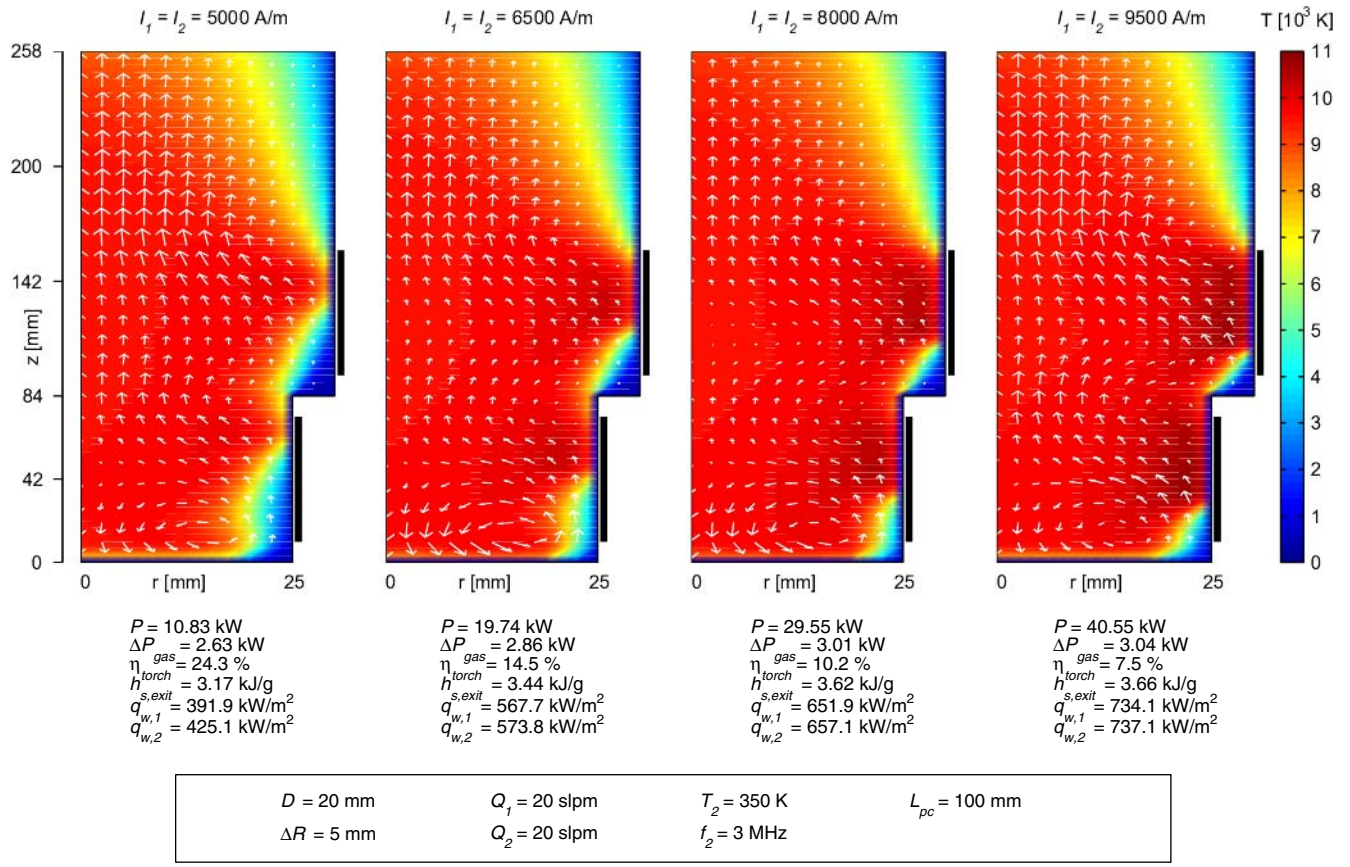

Fig. 19. Plasma temperature and velocity fields for the RF–RF hybrid torch with different values of I_1 and I_2.

hardly support values higher than 600 kW/m^2. On the contrary, the radial profile of plasma temperature at the exit of the torch is only negligibly affected by an increase in f_2 over $f_2 = 3$ MHz (Fig. 18b). The same problem may arise when the electric configuration of the hybrid devices is characterized by a value of $f_2 = f_1 = 3$ MHz and values of the secondary coil current, I_2, higher than 8000 A/m, as shown in Figure 19, where a comparison of the effects of four electric configurations featuring different values of I_1 and I_2 (being $I_1 \equiv I_2$) is made. Even in these cases the radial profile of plasma temperature near the torch wall (see Fig. 21a for the behaviour at mid-coil) and the power density distribution are strongly affected by the values of parameters I_1 and I_2 (Fig. 20), while ΔP_{gas} (Fig. 18) and, even more, the radial profile of plasma temperature at the exit of the torch (Fig. 21b) are only slightly affected.

The combined effects of changing both the frequency f_2 and the geometric configuration of the RF–RF hybrid torch on P, ΔP_{gas} and η_{torch} have been already pointed out in the abovementioned Table 3.

3.3 Parametric study of gas flow configurations

Also the effect of changing the gas flow configuration on the behaviour of the RF–RF hybrid torch has been investigated by means of three different parameterizations: on the primary gas flow rate (Q_1), on the secondary gas flow rate (Q_2), and on the total gas flow rate ($Q_{tot} = Q_1 + Q_2$, with $Q_1 = Q_2$). Investigations on the effects of the inlet temperature of the secondary gas (T_2) on the behaviour of the RF–RF hybrid torch have also been performed.

Figure 31 graphically summarizes the way P, ΔP_{gas} and η_{torch} are affected by variations in Q_1 and Q_2, for a hybrid torch characterized by the geometrical and electrical parameters whose values are given in the caption of the figure. The value of the primary gas flow rate, Q_1, affects P, ΔP_{gas} and η_{torch} as a result of its strong influence on the power density distribution and on the plasma temperature and flow fields. This influence is shown in Figures 22 and 23 for a RF–RF hybrid torch with geometrical and electrical configuration as the one of Figure 31 and with Q_2 fixed at 20 slpm. The higher the value of Q_1, the higher the radial confinement of the high temperature region of the discharge, leading to a decrease in the plasma temperature at mid-coil of the secondary stage in the region close to the wall of the confinement tube (Fig. 24a), as well as a decrease in the heat fluxes through the wall of the confinement tube of both the primary and secondary stages of the hybrid device ($q_{w,1}$ and $q_{w,2}$, respectively, whose maximum values are given in Fig. 22). Also the magnitude of the axial component of the plasma velocity increases when Q_1 increases (see Fig. 23). However, at the same time, the plasma temperature radial profile at the torch exit is only slightly affected by changes in Q_1 (see Fig. 24b).

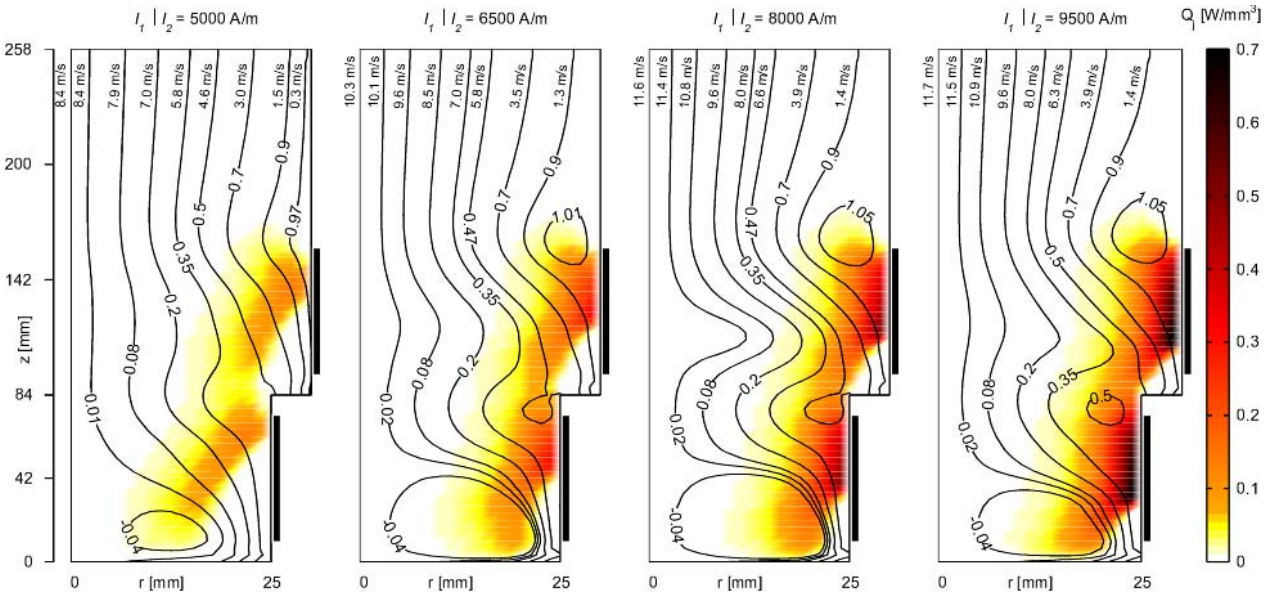

Fig. 20. Power density distributions and streamline patterns, with corresponding axial components of gas velocity at the exit of the RF–RF hybrid torch, for the cases of Figure 19.

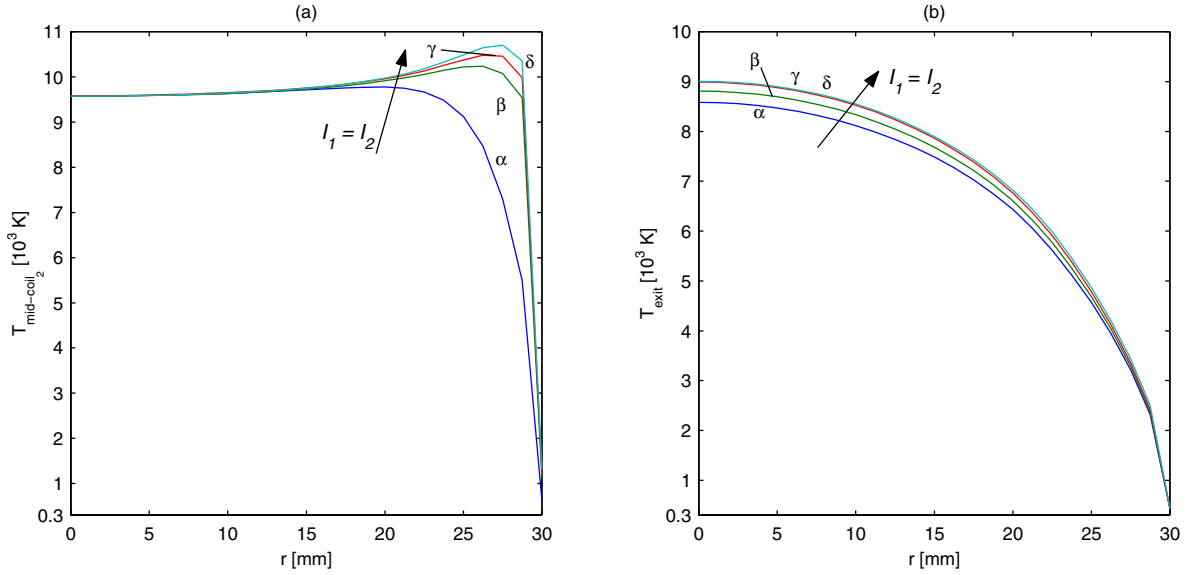

Fig. 21. Radial profiles of plasma temperature at mid-coil of the secondary stage (a) and at the torch exit (b) for the cases of Figure 19: (α) $I_1 = I_2 = 5000$ A/m; (β) $I_1 = I_2 = 6500$ A/m; (γ) $I_1 = I_2 = 8000$ A/m; (δ) $I_1 = I_2 = 9500$ A/m.

Results in Figures 22 and 31 show a monotonically decreasing behaviour of η_{torch} for increasing values of Q_1 as a consequence of a decrease in P and of an increase in ΔP_{gas}. Plasma temperature, flow fields and power density distributions in four different configurations with Q_2 varying from 20 slpm to 150 slpm, are given in Figures 25 and 26, for a case with the same geometrical and electrical configuration as that of the case reported in Figure 31 and with $Q_1 = 20$ slpm. From the results reported in Figures 25 and 26, one can appreciate that a change in Q_2 has negligible impact on the fluid-dynamics of the primary stage of the RF–RF hybrid torch, while it strongly affects the characteristics of the secondary stage. Additionally, as Q_2 increases, the plasma temperature in the region close to the confinement tube at mid-coil of the secondary stage decreases (Fig. 27a), inducing a decrease of the heat flux through the wall of the secondary stage, whose maximum values, $q_{w,2}$, are given in Figure 25; the heat flux through the wall of the primary stage, as expected, remains mainly unaffected by the increase in Q_2. Figure 27b shows that also the temperature profiles at the torch exit is affected by a change in Q_2, for the whole region where streamlines related to Q_2 are to be considered (see Fig. 26). It is worth noticing (Fig. 25) that a change in Q_2 always affects on $h_{s,exit}$ (the reason lies in the definition of $h_{s,exit}$ itself), but the impact of an increase in Q_2 on

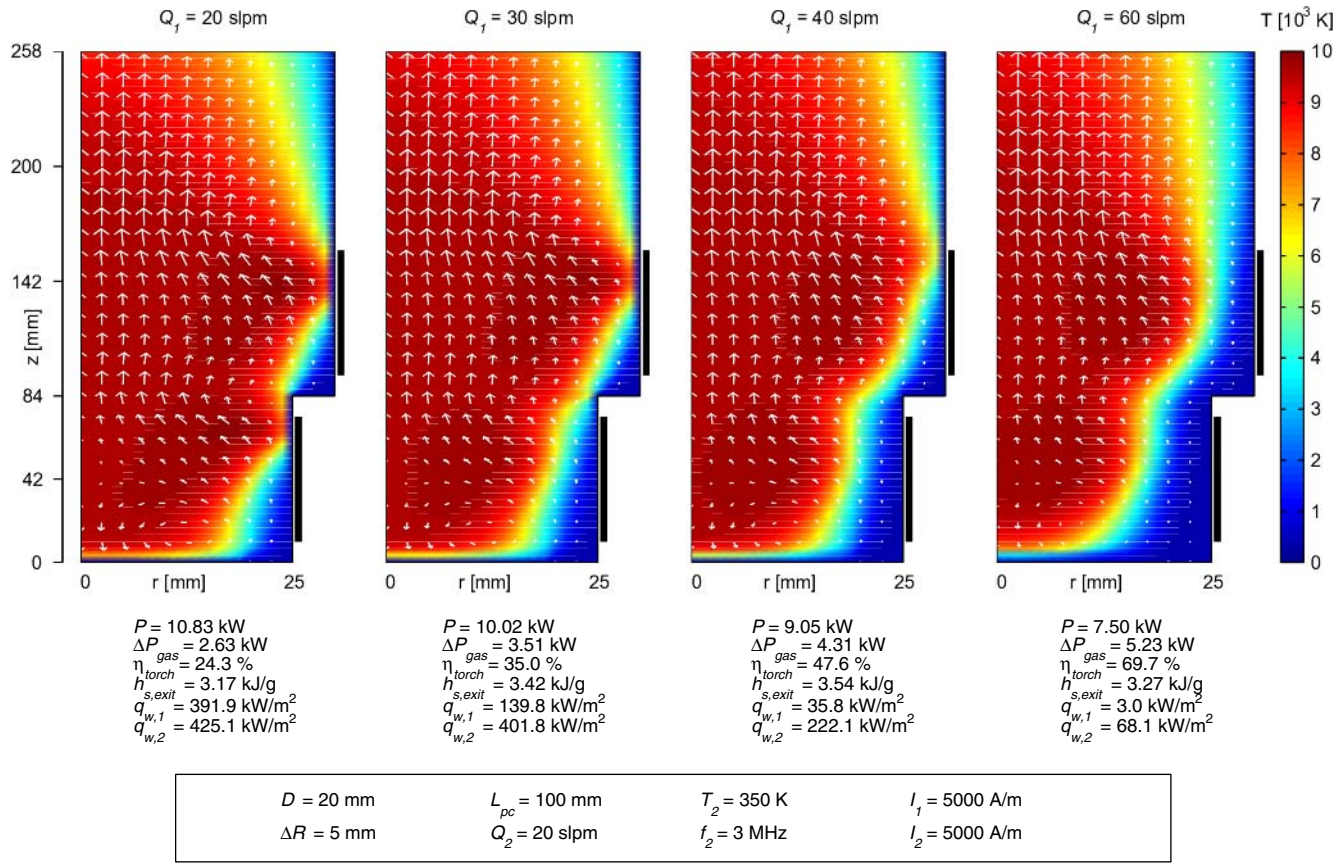

Fig. 22. Plasma temperature and velocity fields for the RF–RF hybrid torch with different values of Q_1.

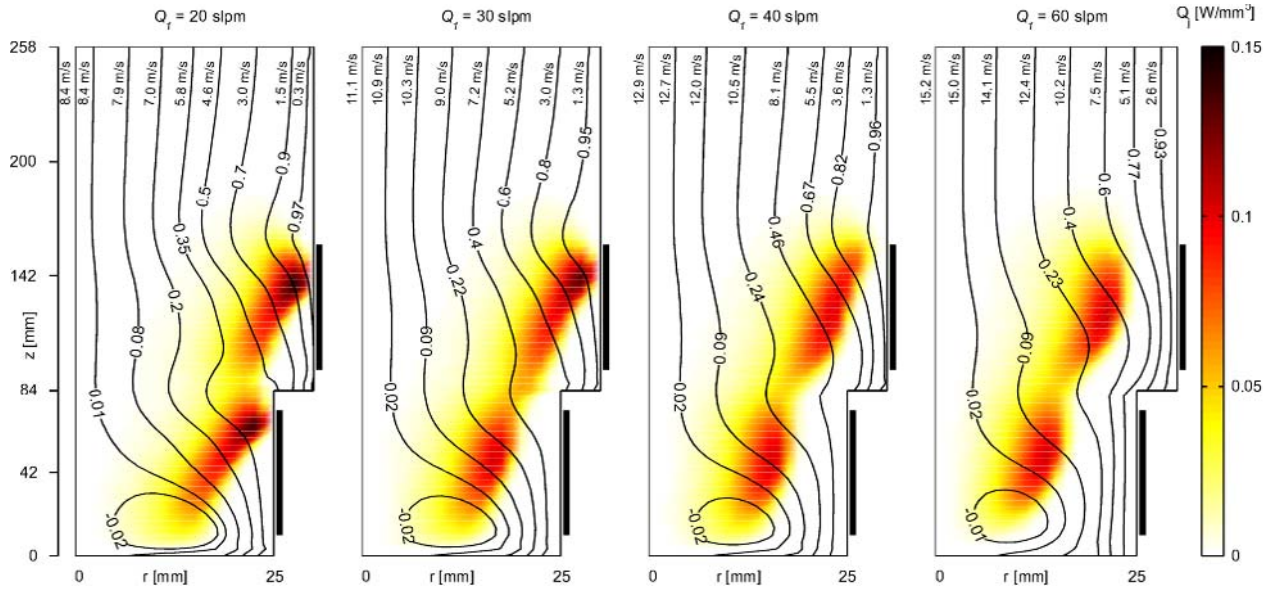

Fig. 23. Power density distributions and streamline patterns, with corresponding axial components of gas velocity at the exit of the RF–RF hybrid torch, for the cases of Figure 22.

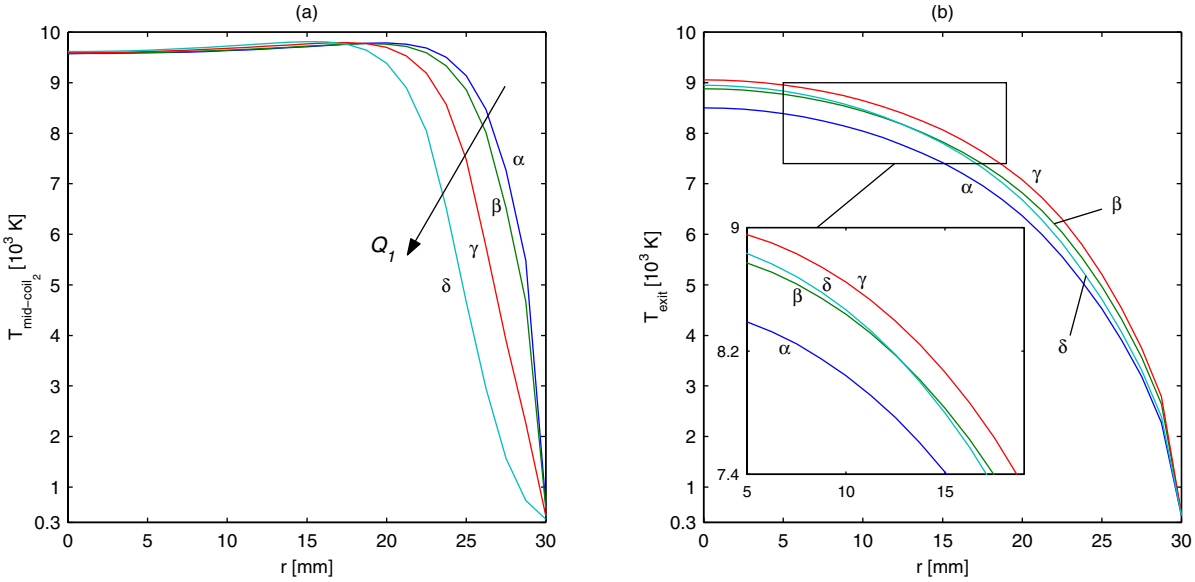

Fig. 24. Radial profiles of plasma temperature at mid-coil of the secondary stage (a) and at the torch exit (b) for the cases of Figure 22: (α) $Q_1 = 20$ slpm; (β) $Q_1 = 30$ slpm; (γ) $Q_1 = 40$ slpm; (δ) $Q_1 = 60$ slpm.

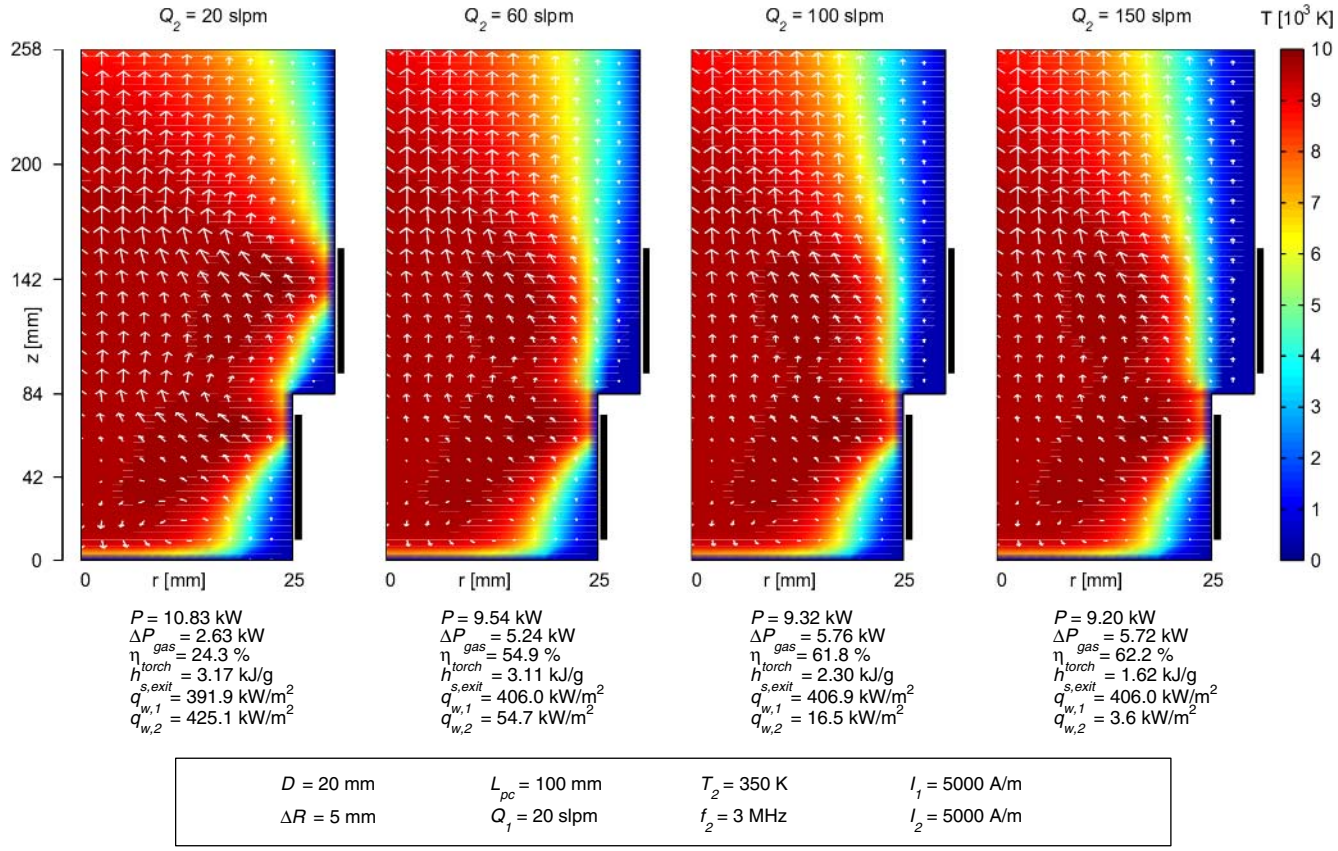

Fig. 25. Plasma temperature and velocity fields for the RF–RF hybrid torch with different values of Q_2.

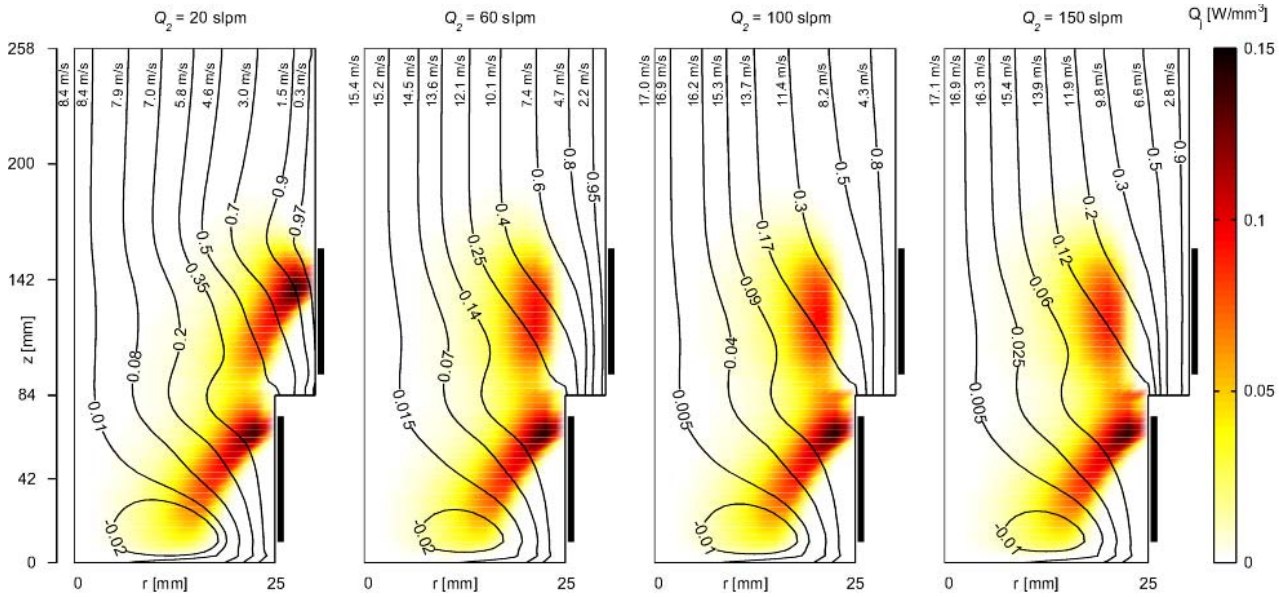

Fig. 26. Power density distributions and streamline patterns, with corresponding axial components of gas velocity at the exit of the RF–RF hybrid torch, for the cases of Figure 25.

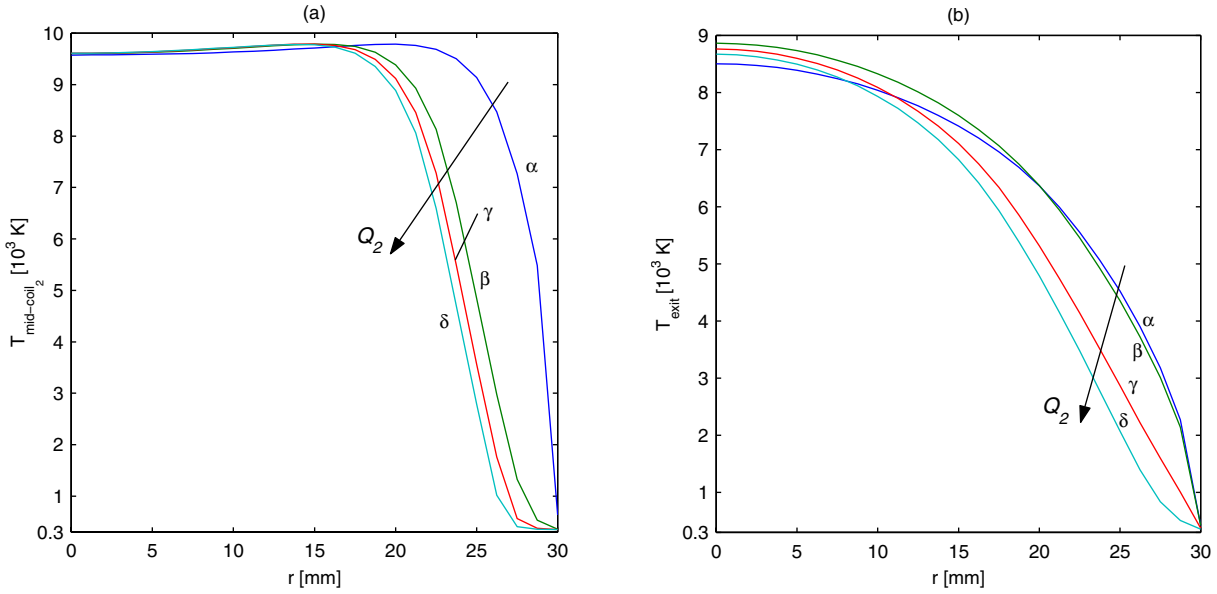

Fig. 27. Radial profiles of plasma temperature at mid-coil of the secondary stage (a) and at the torch exit (b) for the cases of Figure 25: (α) $Q_2 = 20$ slpm; (β) $Q_2 = 60$ slpm; (γ) $Q_2 = 100$ slpm; (δ) $Q_2 = 150$ slpm.

the discharge power P, on the radial extension of the high temperature region of the discharge, and on the plasma temperature and flow fields, become less and less important as Q_2 increases. Both Figures 25 and 26 support this conclusion. With the final aim of somehow widening the content of information of the parametric study related to Q_2 with respect to what has been presented in Figure 25 for $D = 20$ mm, a sample of the effect on P, ΔP_{gas} and η_{torch} of changing the secondary gas flow rate, Q_2, is shown in Figure 33, also for three geometric configurations characterized by different values of D (the values of the gas flow and electric parameters are given in the figures' caption).

Conclusions can be drawn from Figure 33 concerning a strong monotonically decrease of ΔP_{gas} for increasing values of D in the range of high flow rate Q_2. A torch geometry with intermediate coupling ($D = 100$ mm) induces values of η_{torch} higher than the ones obtainable with $D = 20$ mm and $D = 186$ mm, for the whole range of spanning of Q_2 here taken into account. Comparison of results for $D = 20$ mm and $D = 186$ mm shows the existence of an inversion point at $Q_2 \backsim 40$ slpm for what concerns the best value of η_{torch}.

The parameterization on the total gas flow rate ($Q_{tot} = Q_1 + Q_2$) has been performed under the assumption $Q_1 = Q_2$. In Figures 28, 29 and 30, the gas flow

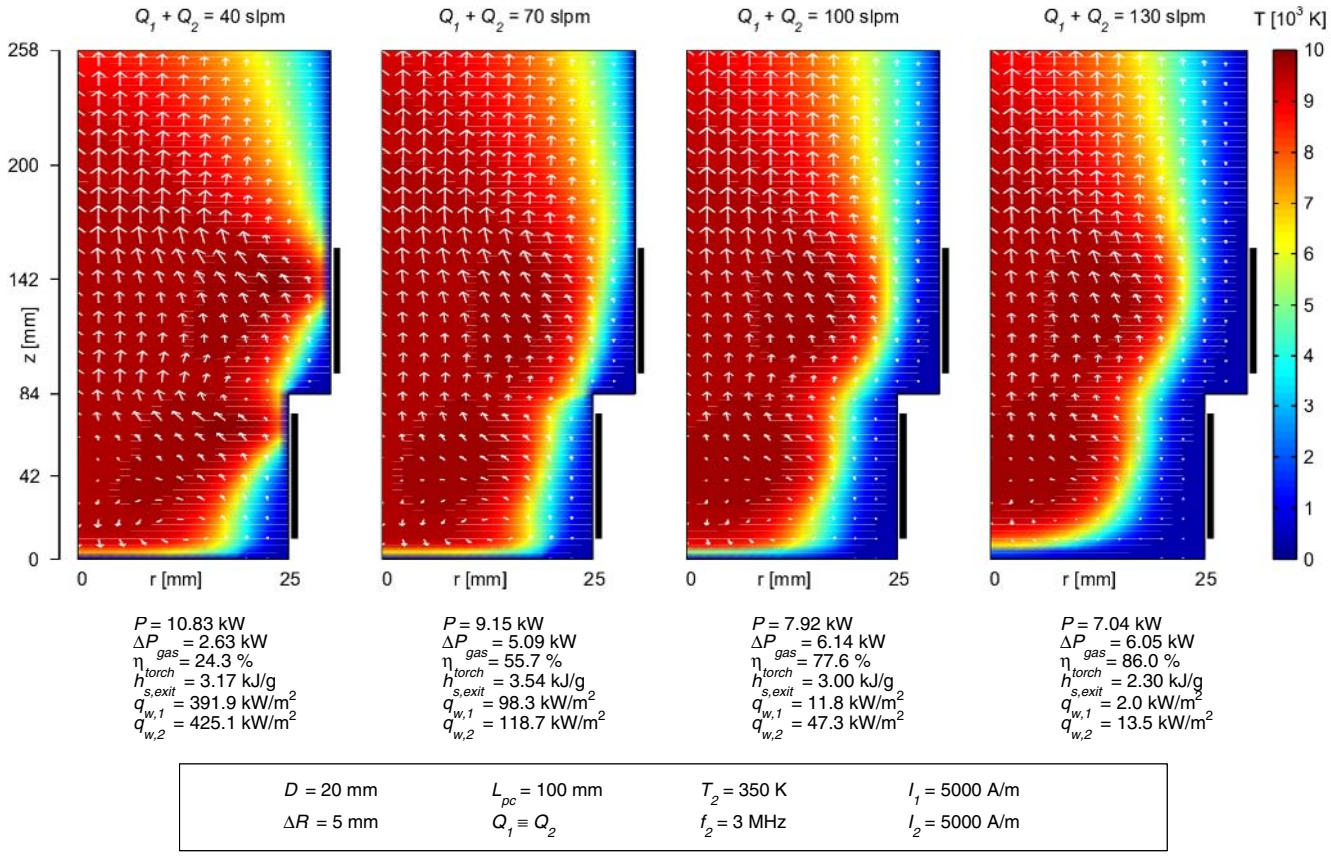

Fig. 28. Plasma temperature and velocity fields for the RF–RF hybrid torch with different values of $Q_1 + Q_2$.

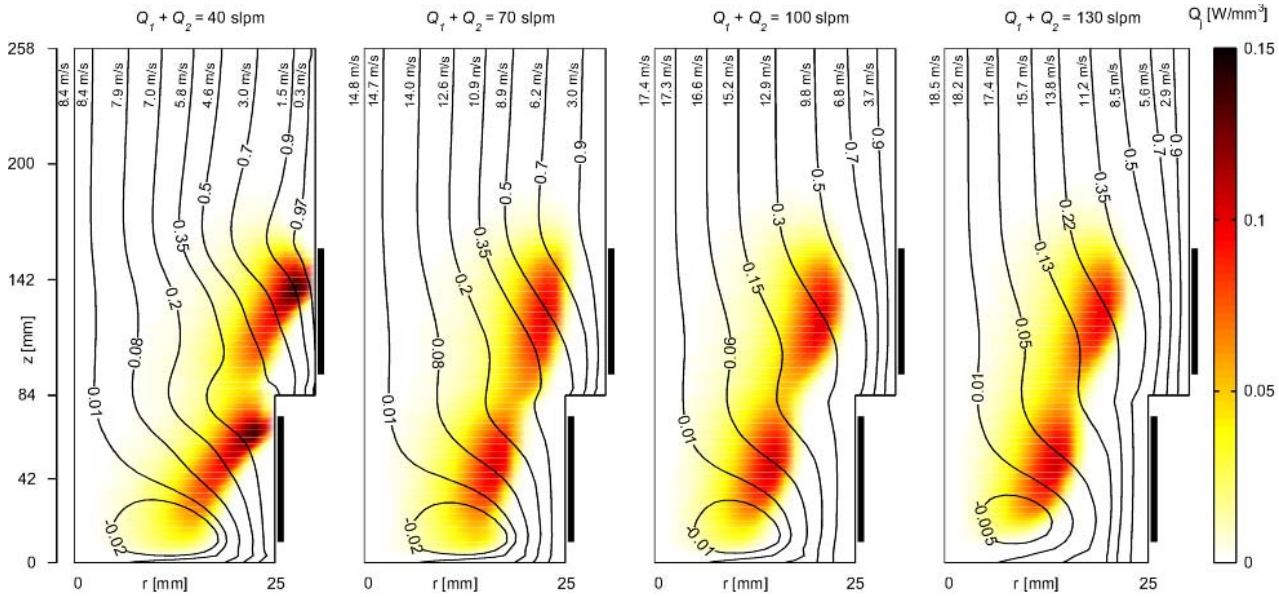

Fig. 29. Power density distributions and streamline patterns, with corresponding axial components of gas velocity at the exit of the RF–RF hybrid torch, for the cases of Figure 28.

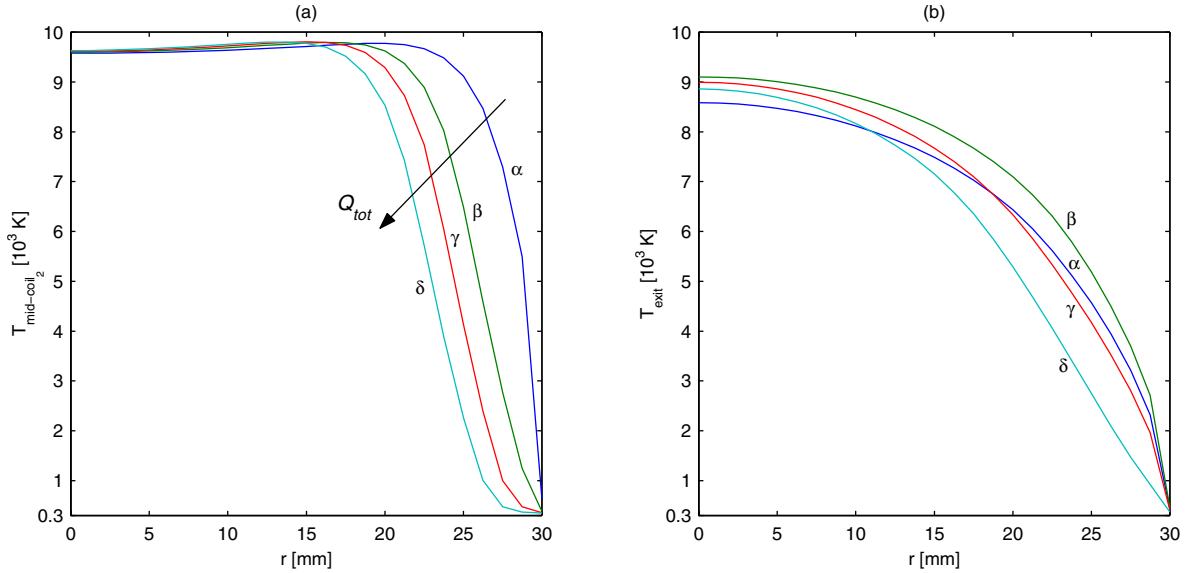

Fig. 30. Radial profiles of plasma temperature at mid-coil of the secondary stage (a) and at the torch exit (b) for the cases of Figure 28: (α) $Q_1 + Q_2 = 40$ slpm; (β) $Q_1 + Q_2 = 70$ slpm; (γ) $Q_1 + Q_2 = 100$ slpm; (δ) $Q_1 + Q_2 = 130$ slpm.

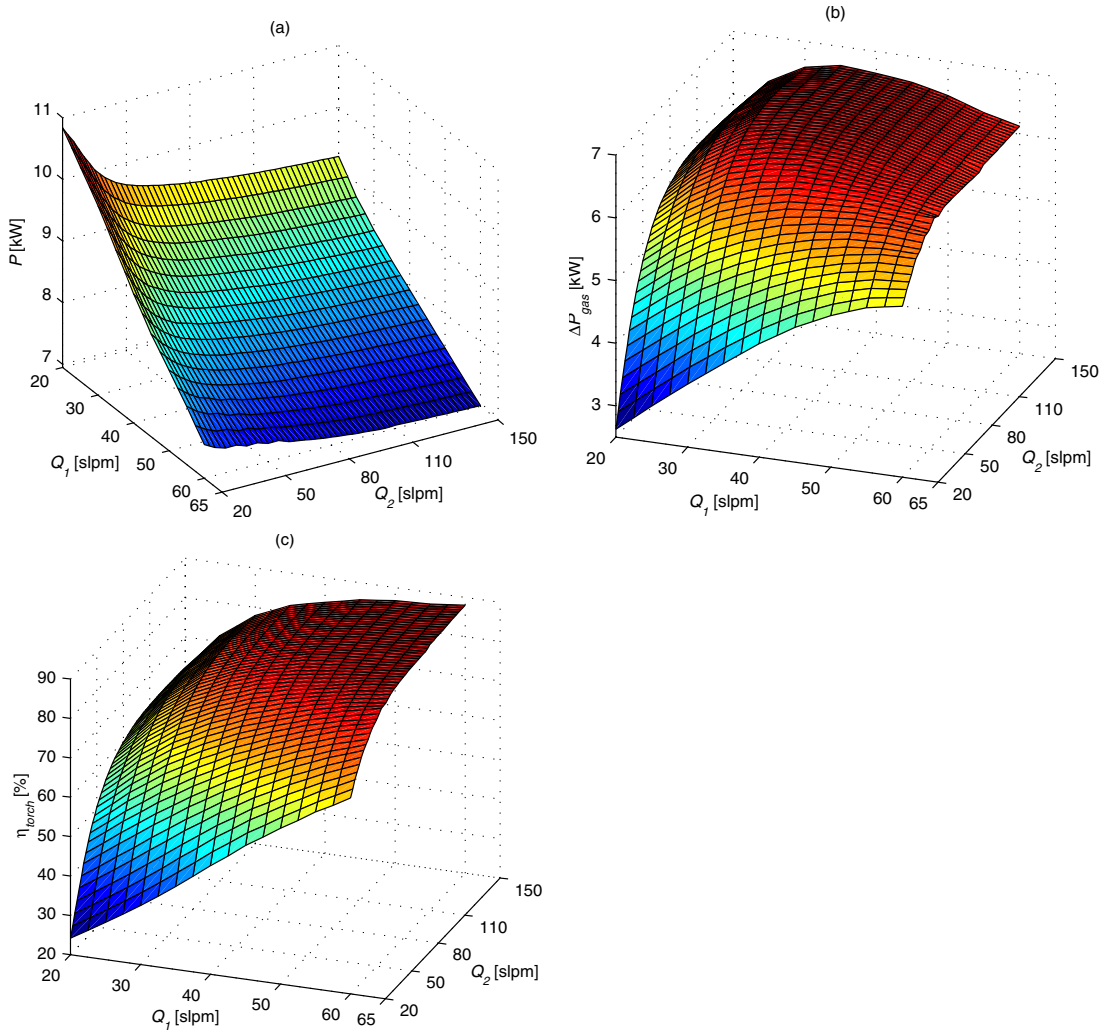

Fig. 31. Effect of changing Q_1 and Q_2 on P (a), ΔP_{gas} (b), η_{torch} (c), for the RF–RF hybrid torch with the following operating conditions and geometric configuration: $D = 20$ mm, $\Delta R = 5$ mm, $I_1 = I_2 = 5000$ A/m, $f_2 = 3$ MHz, $T_2 = 350$ K, $L_{pc} = 100$ mm.

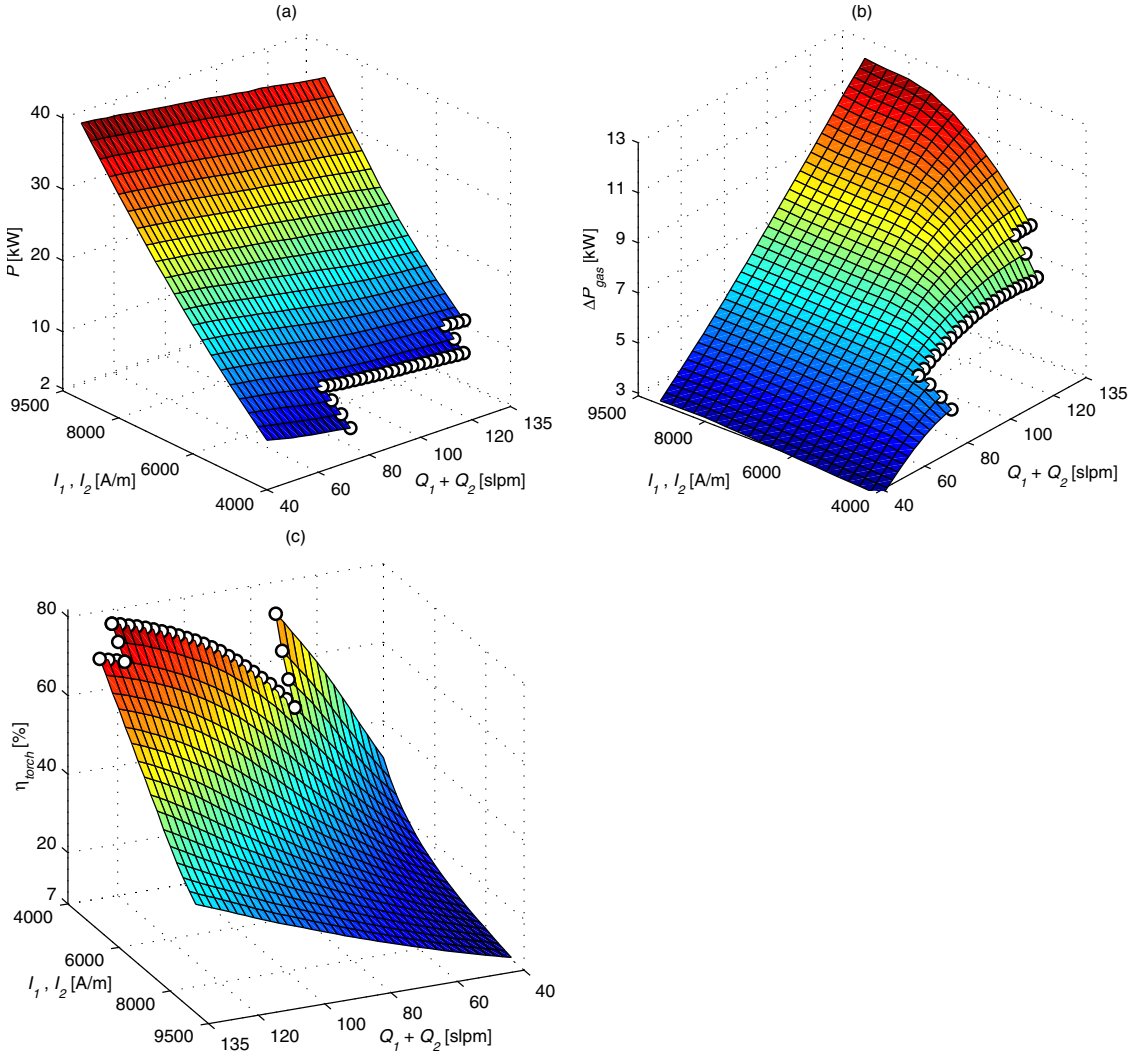

Fig. 32. Effect of changing I_1, I_2 and $Q_1 + Q_2$ on P (a), ΔP_{gas} (b), η_{torch} (c), for the RF–RF hybrid torch with the following operating conditions and geometric configuration: $D = 20$ mm, $\Delta R = 5$ mm, $I_1 = I_2$, $f_2 = 3$ MHz, $Q_1 = Q_2$, $T_2 = 350$ K, $L_{pc} = 100$ mm. The symbol ∘ indicates the limit of sustainability for the secondary plasma.

configuration with $Q_{tot} = 40$ slpm ($Q_1 = Q_2 = 20$ slpm; corresponding, accordingly with Fig. 22, to $\eta_{torch} = 24.3\%$) is compared with three different gas flow configurations obtained increasing Q_{tot} up to 130 slpm, for a strongly coupled configuration with small ΔR, fully described in the caption of Figure 28. The main effects of an increase in Q_{tot} are a simultaneous decrease in P and an increase in η_{torch} (which reaches values close to 86% for the configuration with $Q_{tot} = 130$ slpm). An increase in Q_{tot} induces a strong confinement of the discharge towards the axis of the torch and a decrease of the maximum values of the heat flux to the wall of both the primary and secondary stage of the RF–RF hybrid torch ($q_{w,1}$ and $q_{w,2}$, respectively). Also the effects of increasing the total gas flow rate, Q_{tot}, on the plasma temperature profiles at mid-coil of the secondary stage and at the torch exit (Fig. 30) are similar to those previously discussed in Figures 24 and 27, and may be explained with similar arguments. Figures 23, 26 and 29 show a similar behaviour for what concerns the gas velocity distribution at the exit of the torch.

In order to investigate the effects on the secondary plasma sustainability of the value of the total gas flow rate and of the value of the linear coil current densities I_1 and I_2 (with $I_1 = I_2$), results for P, ΔP_{gas} and η_{torch} are summarized in Figure 32 for a wide spanning range of these parameters. The black-edged white circles appearing on the surfaces of Figure 32 indicate the limit of sustainability for the secondary plasma.

In conclusion, also the effect on the behaviour of the RF–RF hybrid torch of changing the inlet temperature of the secondary gas, T_2, (taking into account the possibility of a preprocessing occurring to the secondary gas) has also been numerically investigated, for various torch geometries and operating conditions ($f_2 = 2 \div 4.5$ MHz; $Q_2 = 20 \div 60$ slpm; $T_2 = 350 \div 2000$ K). For the sake of conciseness, results will not be presented here, since

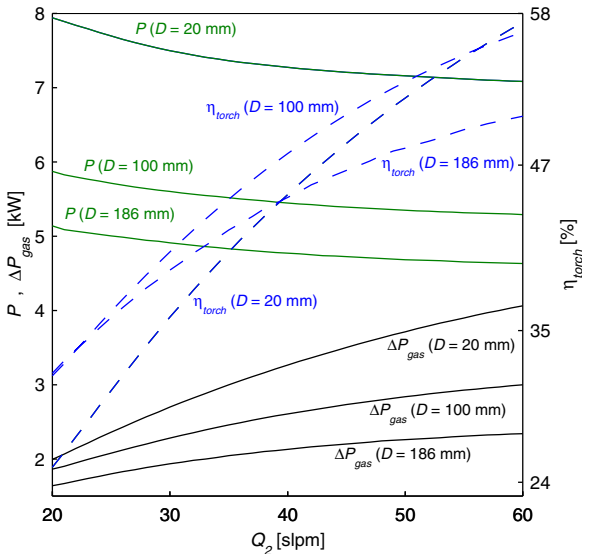

Fig. 33. P, ΔP_{gas} and η_{torch} as functions of the secondary gas flow rate Q_2 for different values of D, for the RF–RF hybrid torch with $\Delta R = 5$ mm, $I_1 = 4600$ A/m, $I_2 = 4300$ A/m, $f_2 = 3$ MHz, $Q_1 = 20$ slpm, $T_2 = 350$ K, $L_{pc} = 100$ mm.

they show an almost negligible dependency of discharge power P and η_{torch} on a change in T_2.

4 Conclusions and future developments

A two-dimensional, fluid-magnetic code has been developed to simulate the physical behaviour of RF–RF hybrid plasma torches, taking into full account also the electromagnetic interaction between the primary and secondary induction stages, with the final aim of defining the potentialities of this type of device in a wide range of operating conditions that may be interesting for particular industrial applications, for which suitable design strategies are to be used. Calculations have been carried out to investigate the influence on the main plasma properties of different geometrical, electrical and gas flow operating conditions.

The results show that the energy efficiency of the torch, η_{torch}, may be higher than in conventional torches, although the technological problems that could arise due to the system intrinsic complexities (in particular the ones related to primary and secondary coil interactions and electric supply) have not been taken into account within the frame of numerical simulations.

Radial injection of a carrier gas in the secondary stage of the RF–RF hybrid torch [3] has not been taken into account yet and experiments on some of the configurations here presented should be accomplished, both to validate simulation results and to test the technical feasibility of the RF–RF hybrid systems for those configurations which were not considered in the past by other researchers.

In conclusion it must be said that the results presented in this work in terms of η_{torch} should be analysed case by case matching the numerical model for the RF–RF hybrid torch with a fully integrated model that would take into account the real complexity of the electric circuits generating the RF power and the coupling efficiency between generator and plasma; this would finally account for a form factor modifying both appearance and values of the η_{torch} surfaces as function of suitable couples of geometric, electric and gas flow parameters.

This work was performed with partial financial support from the University of Bologna Goal-Oriented project 2001–2003 and ex-60% 2001–2002 projects, from the Italian Ministry of Education, University and Scientific Research (MIUR) national project COFIN 2002 and National Group for Mathematical Physics (GNFM) of the Italian Institute of High Mathematics. The Authors wish to gratefully thank Prof. M.I. Boulos for the useful discussions on the subject matter of this paper.

References

1. T. Kameyama, K. Jukuda, Development of an all solid state r.f.-r.f. induction plasma system, 30 kW, 1–15 MHz, Nat. Chem. Lab. Indust. Int. Rep. **21**, 4 (1986)
2. J.W. McKelliget, N. El–Kaddah, J. Appl. Phys. **64**(6), 2948 (1988)
3. T. Uesugi, O. Nakamura, T. Yoshida, K. Akashi, J. Appl. Phys. **64**(8), 3874 (1988)
4. T. Kameyama, K. Sakanaka, A. Motoe, T. Tsunoda, T. Nakanaga, N.I. Wakayama, H. Takeo, K. Fukuda, J. Mater. Sci. **25**, 1058 (1990)
5. M.I. Boulos, High Temp. Mater. Proc. **1**(1), 17 (1997)
6. T. Yoshida, K. Nakagawa, T. Harada, K. Akashi, Plasma Chem. Plasma Proc. **1**(1), 113 (1981)
7. A. Gutsol, J. Larjo, R. Hernberg, Plasma Chem. Plasma Proc. **22**(3), 351 (2002)
8. T. Yoshida, T. Tani, H. Nishimura, K. Akashi, J. Appl. Phys. **54**(2), 640 (1983)
9. J.W. McKelliget, N. El–Kaddah, Metallurg. Trans. B **21**, 589 (1990)
10. V. Colombo, C. Panciatichi, A. Zazo, G. Cocito, L. Cognolato, IEEE Trans. Plasma Sci. **25**(5), 1073 (1997)
11. D. Bernardi, V. Colombo, G.G.M. Coppa, A. D'Angola, Eur. Phys. J. D **14**, 337 (2001)
12. J. Kim, J. Mostaghimi, R. Iravani, IEEE Trans. Plasma Sci. **25**, 1023 (1997)
13. A. Merkhouf, M.I. Boulos, Plasma Sources Sci. Technol. **7**, 599 (1998)
14. A. Merkhouf, M.I. Boulos, J. Phys. D: Appl. Phys. **33**, 1581 (2000)
15. D. Bernardi, V. Colombo, G.G.M. Coppa, E. Ghedini, A. Mentrelli, Investigation on Operating Conditions and Efficiency Optimization of RF–RF Hybrid Plasma Torches, in *Progress in Plasma Processing of Materials, Proceedings of the 6th International Thermal Plasma Processing Conference (TPP–6)*, Strasbourg (France), May 30–June 2, 2000, pp. 359–364, edited by P. Fauchais (New York–Wallingford, Begell House, 2001)
16. D. Bernardi, V. Colombo, G.G.M. Coppa, E. Ghedini, A. Mentrelli, Numerical Modelling of RF–RF Hybrid Plasma Torches and Parametric Study for Various Geometric, Flow and Electric Configurations, in *Progress*

in Plasma Processing of Materials, Proceedings of the 6th International Thermal Plasma Processing Conference (TPP–6), Strasbourg (France), May 30–June 2, 2000, pp. 339–346, edited by P. Fauchais (New York–Wallingford, Begell House, 2001)

17. D. Bernardi, V. Colombo, G.G.M. Coppa, E. Ghedini, A. Mentrelli, Parametric Study on Operating Conditions and Energy Efficiency for Two-Stage Hybrid RF–RF and One-Stage Modified-Coil RF Plasma Torches, in *Proceedings of 15th International Symposium on Plasma Chemistry (ISPC–15)*, Orléans, France, 9–13 July 2001, edited by GREMI, CNRS/University of Orléans, pp. 161–166
18. D. Bernardi, V. Colombo, G.G.M. Coppa, E. Ghedini, A. Mentrelli, Non Conventional Design of Inductiveley Coupled Plasma Torches for Industrial Applications, XV Congresso Nazionale sulla Scienza e Tecnologia del Vuoto, Lecce, Italy, May 17–19, 2000; Vuoto - scienza e tecnologia, **XXIX**, 3/4, 46–51 (2000)
19. S.V. Patankar, *Numerical Heat Transfer and Fluid Flow* (New York, Hemisphere, 1980)
20. Z. Njah, J. Mostaghimi, M.I. Boulos, Int. J. Heat Mass Transfer **36**, 16 (1983)
21. J. Mostaghimi, P. Proulx, M.I. Boulos, Plasma Chem. Plasma Proc. **4**, 3 (1984)